Journal of Nanostructure in Chemistry (2018) 8:255–291
https://doi.org/10.1007/s40097-018-0278-1

REVIEW

A review on the progress of nanostructure materials for energy harnessing and environmental remediation

Ankita Rani[1] · Rajesh Reddy[1] · Uttkarshni Sharma[1] · Priya Mukherjee[1] · Priyanka Mishra[1] · Aneek Kuila[1] · Lan Ching Sim[2] · Pichiah Saravanan[1]

Received: 6 July 2018 / Accepted: 20 August 2018 / Published online: 3 September 2018
© The Author(s) 2018

Abstract

The nanostructured materials offer various advantages as they provide more flexible space for ease reconstruction, as their nanosize expands the limits and results in confinement effect, enhanced mechanical stability, and large surface area, and make them suitable for photocatalytic activities. The advancement in synthesis techniques provides the freedom to alter its physical properties as per the demand. This article provides a 360° view point on the nanomaterials which are used for solar energy harnessing with respect to environmental and energy application. The discussion emphasizes on various synthesis methods of nanostructured materials, their mechanistic features, usage in demanding applications such as photosplitting of water for hydrogen production, artificial photosynthesis, and water and wastewater treatment with an endnote highlighting the future scope of nanomaterials for real-world applications.

Ankita Rani, Rajesh Reddy, Uttkarshni Sharma, Priya Mukherjee, Priyanka Mishra, Aneek Kuila, and Sim Lan Ching have contributed equally.

✉ Pichiah Saravanan
pichiahsaravanan@gmail.com

[1] Environmental Nanotechnology Laboratory, Department of Environmental Science and Engineering, Indian Institute of Technology (ISM), Dhanbad, Jharkhand 826004, India

[2] Department of Chemical Engineering, Lee Kong Chian Faculty of Engineering and Science, Universiti Tunku Abdul Rahman, Jalan Sungai Long 9, Bandar Sungai Long, 43000 Kajang, Malaysia

Graphical abstract

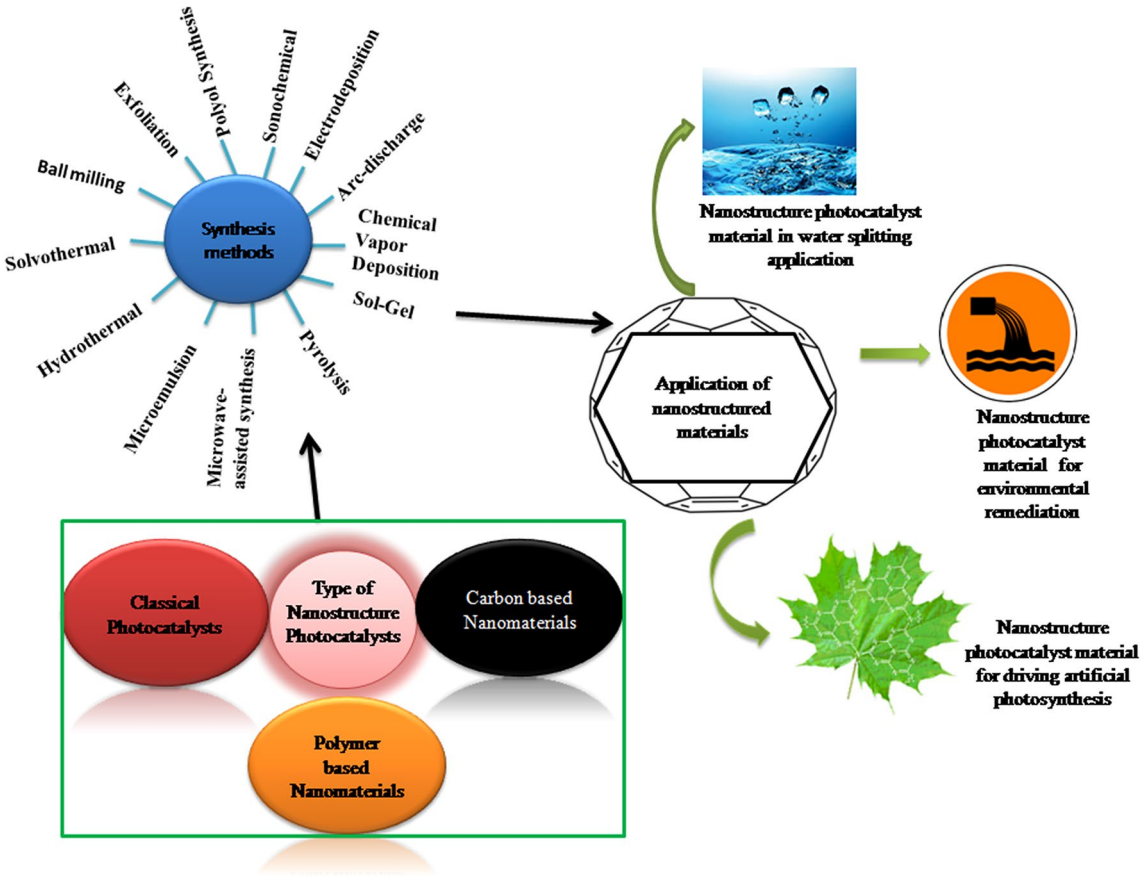

Keywords Nanostructure · Synthesis · Mechanistic features · Water splitting reaction · CO_2 reduction · Water treatment

Introduction

The drastic increment in global population has led to a large increase in energy and water demand. In most cases, the classical energy resources, i.e., fossil fuel, are widely deployed; however, they are prone to release large amount of greenhouse gases as their end product. Being a classical route of combustion, it is impossible to avoid these unwanted gaseous products but prolong release of these gases on the Earth's atmosphere leads to long term effects like global warming and climate change [1, 2]. Moreover, the non-replenishable nature, limited availability, and environmental deterioration caused by processing these fossil fuels urged to search new source of sustainable energy. The natural resources like solar, wind, hydrothermal, and geothermal are some of the well known as they are replenishable and emission free. Among them, solar energy is most preferred, because, besides generating electricity, it can also benefit in water and wastewater treatment, hydrogen production, and driving artificial photosynthesis [1–4].

"Photocatalysis" is a general term which is used for all the catalysis processes which are light driven in nature that uses special category of materials called "Photocatalysts" [5]. Semiconductor is the major category of materials which are chosen for this owing to its electronic structure and intrinsic nature which makes them suitable for this purpose. When the incident light possesses energy greater than bandgap, it excites the electrons of the photocatalyst from the valence band (VB) to the conduction band (CB) leading to the generation of holes in VB. During the aqueous phase reaction, the generated holes oxidize water molecule, thus leading to the production of O_2 in the VB, whereas electrons in the CB reduce the H + ion producing hydrogen. Furthermore, the aquatic phase reaction of electron hole pair results in the production of reactive oxygen species (ROS), a strong oxidant for the degradation of recalcitrant pollutants [2, 4, 5].

Similarly, CO_2 can also be directly photoreduced to methane, methanol, ethanol, acetate, etc., mimicking photosynthesis process. Mineralizing several complex aquatic organic contaminants is one of the unique properties of light-driven materials. Major categories of pollutants that have been successfully removed include textile dyes, phenolic compounds, pesticides, insecticides, aldehydes, pharmaceuticals, health care products, etc. It has been observed that intrinsic modifications such as doping, co-catalyst loading, as well as extrinsic modification such as addition of external electron acceptor can significantly enhance the mineralisation rate of these pollutants under diverse light sources [6–13].

The photocatalytic activity is measured in terms of apparent quantum yield (AQY) which is given by the following equation [14]:

$$\text{AQY}(\%) = (\text{Number of reacted electrons})/(\text{number of incident photons}) \times 100.$$

The quantum yield increases if the photocatalyst is active in visible or near infrared (NIR) region or combination of both, since the amount of solar light reaching the earth surface comprises of ~ 45% visible light and ~ 50% NIR as compared to ~ 5% of ultraviolet light [2, 15].

It is evident that the focus of researchers in the current days is leaning towards nanomaterials as compared to bulk. These nanomaterials possess size range between 1 and 100 nm. Some of the well-known advantages of these nanomaterials are the high surface area-to-volume ratio, improved physical properties (melting point and hardness), and tunable electronic properties [16]. The greater surface area of these nanomaterials allows more space either for storage or reaction. Nanomaterials are harder as compared to that of bulk, because the nanosize prevents the particle from further bending and thus results in increased hardness of the particle. On the other hand, increased hardness results in modification of other physical properties such as malleability, brittleness, ductility, and toughness of the materials. Further reduction of particle size to < 10 nm results in quantum confinement effect and increases the bandgap of the materials, thereby enhancing the charge separation [16, 17]. Moreover, these nanomaterials can be synthesized into morphologies like tubes, rods, flowers, sphere, and many more, while the properties of the specific morphology vary accordingly [18, 19].

Hence, the present review deals with various types of nanostructured photocatalyst to harness solar energy for environmental and energy applications. In specific, the review details the significance of the synthesis, mechanistic feature, application, and future prospect of nanostructured materials.

Type of nanostructure photocatalysts

Classical photocatalysts

In general, the classical photocatalysts refers to inorganic one and includes metal oxides and sulphides. Examples for metal oxide include TiO_2, ZnO, WO_3, V_2O_5, etc., in which TiO_2 is the most widely studied because of its low cost, abundance, non-toxicity, and stability. One of its major disadvantages is the existence of wider bandgap allowing the excitation only in the ultraviolet light range (< 380 nm). However, numerous modifications have been carried out to narrow its bandgap for visible light application [2]. Dopants like N, S, C, Cr^{3+}, Fe^{3+}, V^{5+}, Cu^{2+}, and Ce^{2+} have been used for achieving it [20–44]. In the metal oxide-based semiconductors, the O2p orbital acts as VB maxima, whereas the cationic part acts as CB minima. Moving down to sulphide semiconductors like ZnS, CdS, and SnS_2 have been predominantly studied [45–48]. In this category, the 3p orbital of sulphur that lies at less positive than O2p orbital of metal oxides acts as VB maxima resulting in a narrower bandgap of metal sulphides [2, 15, 45]. Though the metal sulphides are active in visible light, their poor photostability restricts their usage. For an instance, the positive charge carrier in metal sulphide oxidizes their own S^{2-} anion instead of water molecule resulting in photocorrosion [15]. Besides, semiconductors of phosphides (e.g., InP and Ni_2P), selenides (e.g., CdSe, CuSe, ZnSe, etc.), oxynitrides (e.g., TaON), nitrides (e.g., GaN, Ge_3N_4, etc.), phosphates (e.g., Ag_3PO_4), and halides (AgCl and AgBr) origin have been explored [49–65]. The priority on the selection of semiconductors relies on the nature of application. For example, GaN and AgBr are known for their higher photostability, whereas InP for narrow bandgap, i.e., 1.25 eV [49, 59, 65].

Apart from these categories, perovskites have also been widely studied. These photocatalysts possess ABO_3-based crystal structure, which contain two cations A and B, and three oxygen atoms in one molecule. Almost any cations in the periodic table can substitute A and B in the ABO_3 structure, and therefore, their band structure can be easily tuned for desirable photoactivity. These perovskite are highly stable and can be easily synthesized. Some of the well studied in this category includes $SrTiO_3$, $AgNbO_3$, $NaNbO_3$, etc. All these metal oxides, sulphides, and perovskite semiconductors have been widely investigated and applied for water and wastewater treatments in environmental, while for H_2 production and direct CO_2 photoreduction in energy sector [66–68]. Band-gap (Eg) values (in eV) and the edge potential of CB and VB for above-mentioned photocatalysts at pH 0 vs NHE are shown in Fig. 1 [14].

Carbon-based nanomaterials

The predominant electrical, mechanical, and thermal properties of carbon had gained its attraction in various sectors. The widely used carbon-based nanomaterials employed in various energy and environment applications include fullerene and carbon dots of 0D configuration; single and multiwalled carbon nanotubes (CNT) of 1D configuration; graphene, graphene oxide (GO), and reduced graphene oxide (rGO) of 2D configuration [69]. Addition of small percent (~ 1 wt.%) of carbon nanomaterial to semiconductor photocatalysts can enhance their photoactive nature [70]. Materials like CNT, rGO, and fullerene in composite with TiO_2 have shown enhanced photocatalytic activity by increasing the recombination time of charge carriers [70]. This is generally achieved by the preeminent electron capturing and transportation properties contributed by the carbon [70]. Fullerene that is made up of 12 fixed penta rings and varies in number of hexa rings possesses high electron affinity and, hence, is preferred as an electron acceptor [71–73]. Moreover, it is an n-type semiconductor allowing high utilisation of UV light rather than visible [74]. Being an n type, it compliments for the increment of charge carriers and hence used in photocatalysis application [74, 75]. Carbon nanomaterials having size less than 10 nm are categorised as carbon dots (CD) which can be further subclassified as graphene quantum dots (GCD) and carbon nanodots (CND) [76]. The carbon dots possess excellent chemical stability, high specific capacitance, and enhanced luminescence behavior promoting them as excellent photocatalyst with wide applications in energy and environment [77–79]. Their low cost and non-toxic nature along with excellent electron transfer efficacy further substantiate its application [76]. The CNTs have been used in almost every field of energy and environment, either as a catalyst or composite due to its superior electrical conductivity and surface area [80–82]. The physical and chemical properties of CNT enhance the chemical resistance, elasticity, and strength of materials in composite [83]. In general, the low cost and ease availability of graphite has promoted it as an attractive carbon material [84]. It has been widely used in composite with TiO_2 for enhancing its photocatalytic activity. It contributes for the suppression of the charge-carrier recombination and increases the visible photon absorption rate [84]. Graphene, the honeycomb atomic scale lattice of carbon, having properties like high specific surface area and high electrical conductivity is also an alternative active carbon compound to increase the photocatalytic activity of semiconductor photocatalysts [85]. This specific compound in combination with metal oxides has been widely applied in photocatalytic CO_2 reduction, water split reaction, and organic degradation [86–91]. It is

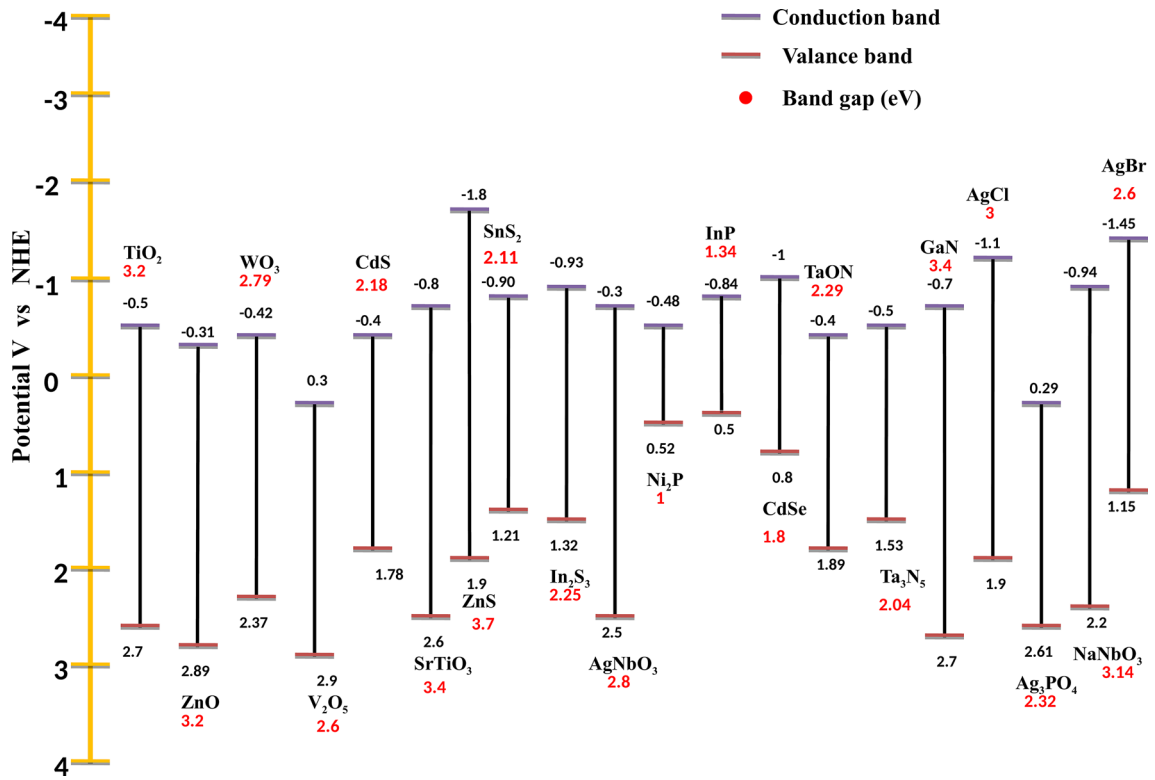

Fig. 1 Schematic depicting Eg values (in eV) and the edge potential of CB and VB at pH 0 vs NHE

also used to synthesize GO which can further synthesize rGO possessing different physical and chemical properties [92]. High surface area and ionisable functional groups of GO craft it as a preferable scaffold in photocatalysis [93]. It would be an ideal support material for photocatalytic water splitting under visible light illumination [94]. Similarly, the layered structure of rGO provides superior site for nucleation and anchors the growth of semiconductor [95]. In specific, it is used in photocatalytic CH_4 production by CO_2 reduction, in Z-scheme water splitting, and water treatment [95–97].

Polymer-based nanomaterials

The conductive polymers have found immense potential to form composites with the various nanomaterials. Polymers like graphitic carbon nitride (g-C_3N_4), polypyrrole (PPy), polyaniline (PANI), polythiophene (PT), polyvinylidene fluoride (PVDF), polyethersulfone (PES), and cellulose have been used in composite with TiO_2 for water purification [98]. In recent years, g-C_3N_4 has been widely used as photocatalyst due to its controllable bandgap, high stability, and low cost [99, 100]. Its bandgap (2.6–2.7 eV) and properties like biocompatibility, chemical stability, and photo resistivity promoted it as a significant visible light photocatalyst [101]. Doping with selected metals or non-metals suppresses the recombination of the charge carriers and further promotes the visible light utilisation [101]. It has been widely employed for H_2 production, CO_2 reduction, and organic pollutant removal [98–102]. It was also found that the conjugated polymers like PPy, PANI, and PT addition enhanced the photocatalytic activity, environmental stability, and photocorrosion resistance [98]. PT incorporation increased the photocatalytic activity by reducing the recombination rate and improving the electron mobility [98]. Having good light absorption property, its composite has been used for H_2 generation [103]. PANI incorporation extended the absorption in the visible light region; similarly, PPy showed good catalytic activity and narrowed the bandgap of the composite [98]. PANI under light irradiation behave as an efficient electron donor and hole transporter, and, hence, used in combination with limited metal oxides [104]. In a study, boron nitride was supported with PANI and thereby applied to remove carcinogenic dyes [104]. The vinylidene fluoride monomers enhance the light contact area of the partnering photocatalyst [105]. Furthermore, the porous structure of the PVDF helps in steady catalyst deposition for improving the photodegradation potential. Moreover, the strong adhering property of PVDF prevents photocatalyst leaching [105]. On the other hand, the ether sulfone network of PES favors photodegradation owing to its robust photostability and high porosity [106–108]. In some recent studies, cellulose, a renewable natural polymer possessing precised structural network with high porosity, is also used as a support for photocatalysts [109, 110]. The presence of hydroxyl group and features like biocompatibility and hydrophilicity favors photocatalysis-mediated water treatment [110].

Modifications in photocatalysts

The modifications in photocatalysts are performed to increase the quantum efficiency of the material. Doping with metals and non-metals, functionalizing with co-catalysts, and formulating binary composites with heterojunction and ternary with an additional co-catalyst are some of the methods adopted to achieve this. These modification techniques are discussed in detail below.

Metal or non-metal doping

This is one of the most familiar and classical techniques to narrow the bandgap of photocatalysts. The narrowing allows the photocatalyst to be active in visible light, thereby enhancing its quantum efficiency. D block metal cations including Nickel, Chromium, Copper, Ruthenium, Ferrous, and Rhodium ions are most commonly considered under metal category, while Carbon, Sulphur, Fluorine, Nitrogen, etc. are considered under non-metal category. Doping with metal ions reduces the bandgap by introducing a new acceptor or donor level within their band structure. The non-metal ions, however, rarely introduce any new impurity level, but they change the valence band potential by shifting it upwards [2, 14]. Figure 2 shows band modification that takes place in photocatalyst when doped with metal or non-metal [2].

Co-catalyst loading

This technique is usually performed for increasing the number of active sites on the surface of the photocatalysts. Most common co-catalysts used are noble metals or metal oxides such as Au, Ag, Pt, Pd, Ru, NiO_x, RuO_x, etc. [2, 4, 111]. Sometimes, these noble metals are covered with a protective coating of chromia (Cr_2O_3) which forms a shell around the co-catalyst for specific reasons. At first, they prevent backward reactions on the surface of the photocatalyst when the noble metals are used as core (i.e., reaction between H_2 and O_2 to form water in the water split reaction). Second, they prevent the metal oxide degradation in the reactant solution when the metal oxides are used as core [112, 113]. Figure 3 illustrates a schematic of the aforesaid mentioned mechanism of shell and core concept [111].

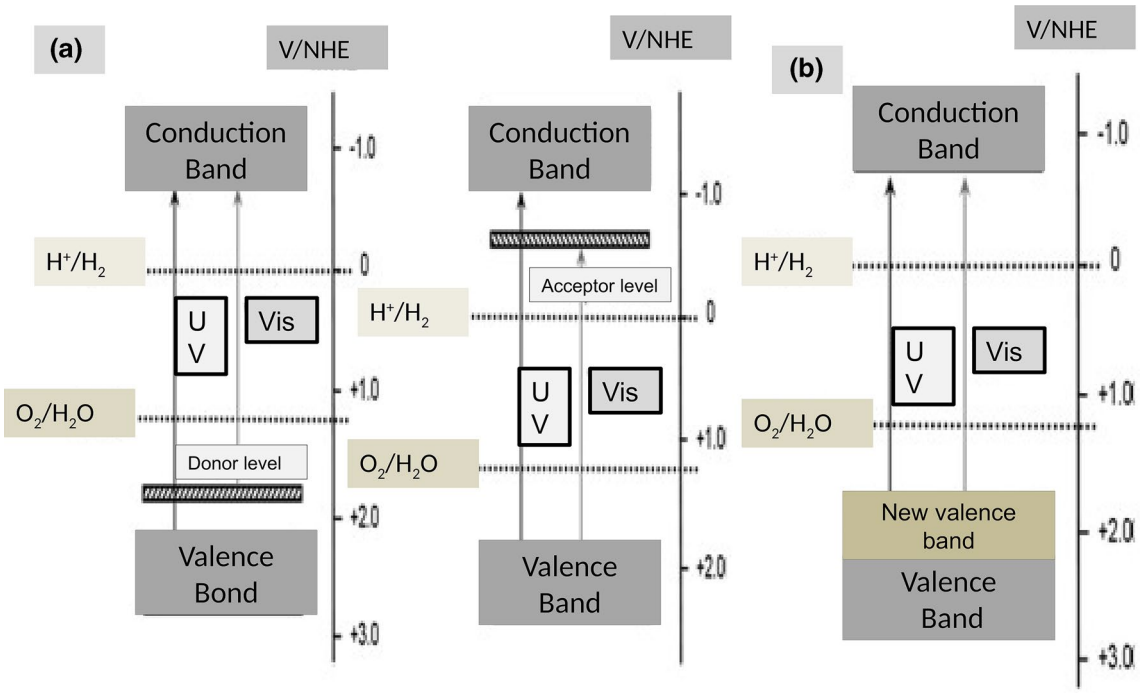

Fig. 2 Schematic showing the impurity level introduced in semiconductors by metal doping (**a**), and upshifting of valence band through non-metal doping (**b**) (the figure is adopted and reproduced with permission from Ref. [2])

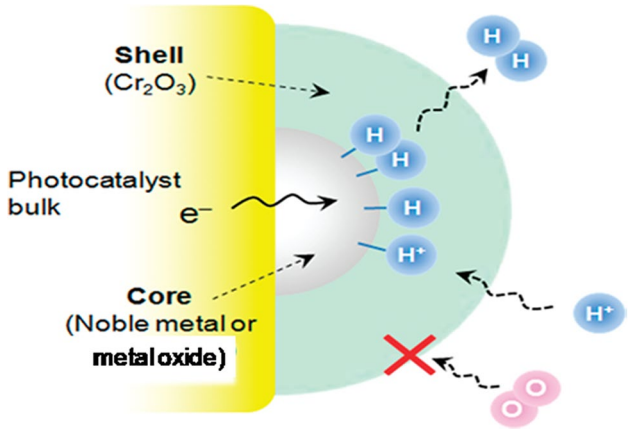

Fig. 3 Schematic showing chromia shell preventing O_2 molecule photoreduction on both noble metal and metal oxide core (the figure is adopted and reproduced with permission from Ref. [111])

Heterojunction structure

These structures are synthesized by coupling two semiconductors whose band structures are aligned in such a way that they allow for enhanced charge separation compared to the single system. Maximum of two alignments are feasible with this binary combination, viz., type I and typeII [3, 114]. A schematic of the band alignment of the nanocomposites for both heterostructures is shown in Fig. 4 [114].

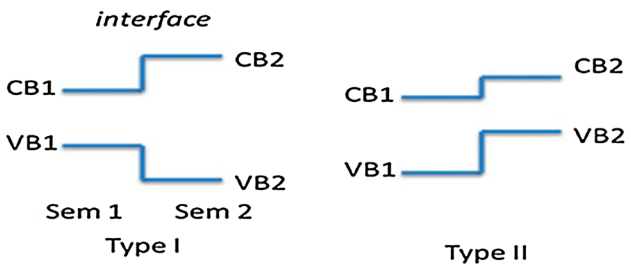

Fig. 4 Band alignment of nanocomposites in type I and II heterostructure (the figure is adopted and reproduced with permission from Ref. [114])

In the type I alignment, both the VB and CB edge potential of either of the semiconductor lies within the bandgap of the other semiconductor as the latter possesses wider bandgap. Since one is having lower VB and CB potentials than the other, therefore, both the bands act as hole and electron collecting sites and are evident from Fig. 5.

Examples of some of the successfully employed type I heterostructure includes CdS/ZnS, BiOCl/BiOI BiOI/TiO_2 heterostructure and few more [115–117]. Considering CdS/ZnS heterostructure, it is a core–shell assembly in which ZnS with wider bandgap forms the shell, while CdS forms the core. The BiOCl/BiOI and BiOI/TiO_2 were of non core–shell assembly in which BiOI was having narrow bandgap, and thus, its edge potential lies within the wider bandgap of BiOCl and TiO_2, respectively.

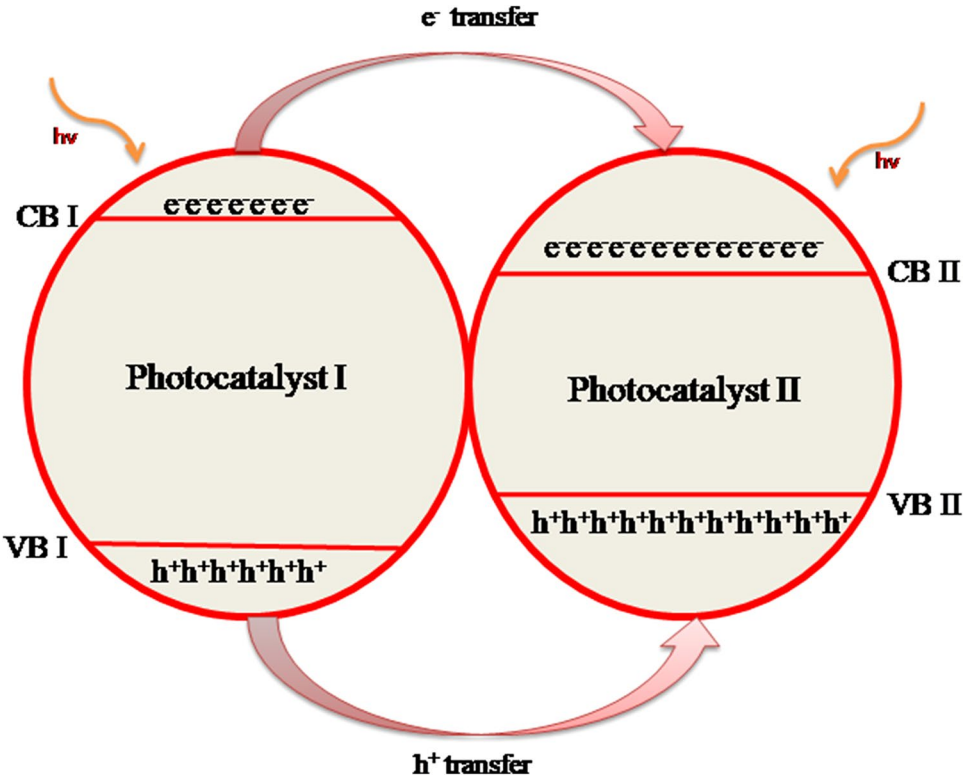

Fig. 5 Schematic showing electron transfer pathway in type I nanocomposite (the figure is adopted and reproduced with permission from Ref. [3])

In the type II heterostructure, CB position of the first semiconductor lies above that of the second, whereas its VB lies within the bandgap of the second. Thus, the photogenerated holes have a tendency to migrate to the VB of first one, whereas the excited electrons have a tendency to migrate to the CB of the second. The first and second implies to the position either of the photocatalyst occupy. The mentioned band position and migration of the charge carriers is depicted in Fig. 6a [4]. In general, the type II heterostructure is widely preferred, because it allows the migration of electrons and holes in opposite direction [3]. On the other hand, an alternative pathway that the electrons can follow is Z-pathway. In this scheme, the electrons after photoexcitation in VB of one semiconductor jump to higher potential CB of the second. The oxidation reaction takes place in the VB of the first semiconductor that is located at higher potential than that of the second [3, 4]. This Z-scheme interaction is pictorially represented in Fig. 6b [4]. Since both the redox reactions are occurring at higher potentials, therefore, the Z-scheme pathway results in higher redox efficiency as compared to the redox efficiency of type II. g-C_3N_4/SnS_2, g-C_3N_4/$NaNbO_3$, Ag_3PO_4/AgI, CdS/WO_3, WO_3/g-C_3N_4, etc. are some successfully synthesized heterostructures that follow either type II or Z-pathway. These have shown good photocatalysis performance for driving direct reduction of CO_2, water split reaction, and wastewater treatment [118–122].

Quantum dots (QDs)

QDs are zero-dimensional semiconductor nanomaterials having particle size close to Bohr radius. QDs possess

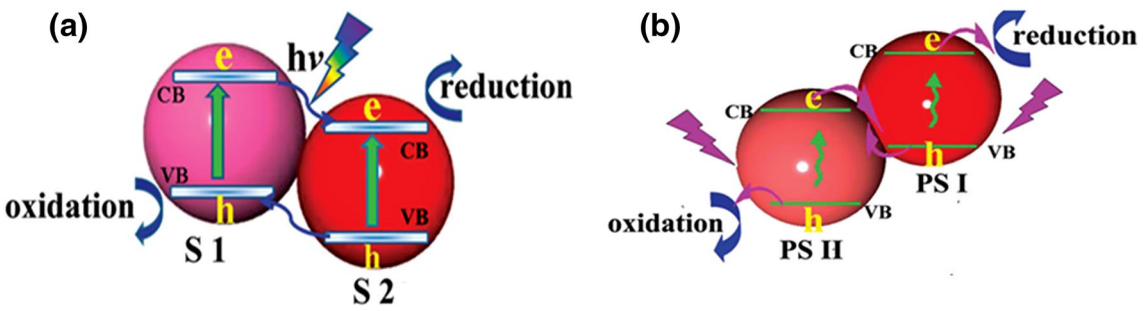

Fig. 6 Heterostructure formed by semiconductors and their electron mobilisation in type II (**a**) and Z scheme (**b**) [4]

comparatively enhanced material properties than usual nanomaterial owing to the confinement of electrons and associated holes. The energy emitted by excited photons in QDs varies according to the semiconductor used and could be adjusted by varying the particle sizes through quantization or quantum size confinement [123, 124]. It appreciably enhances the photostability of the adjoining photocatalyst, increases electron hole separation, and, thus, helps in improving the overall quantum efficiency of the photocatalyst [77]. The carbon QDs (CQDs) in combination with Ag_3PO_4 and Ag showed enhanced visible light photocatalysis with a clear quantum confinement [77]. Therefore, the QDs or CQDs in standalone or in combination with noble metal and photocatalyst of any origin act as an efficient energy material for photocatalysis applications.

Each of the modifications mentioned above are having their own advantages and disadvantages. Doping by the metals or non-metals internally changes the band structure of the photocatalyst which makes them active in the visible region and thus aid in increasing the quantum efficiency, whereas co-catalyst loading increases, the number of active site present on the surface of photocatalyst thus is helpful in increasing the product yield. QDs are quite new in this area and are responsible for the quantum confinement effect which results in changes in several properties of the nanomaterial as well as a better charge separation and stability of the photocatalyst. Furthermore, the application of heterostructures is revolutionizing, since it allows composite consisting of two photocatalysts to be present in a system. Their appropriate band alignment results in better absorption of visible light and charge separation than the single [125, 126].

Synthesis of nanostructure materials

There is a wide variety of synthesis technique available for the synthesis of aforementioned nanostructure materials. However, the selection depends on the need and availability of the method and material for the application. The most commonly adopted synthesis method for some specified energy and environmental applications are discussed below, and their respective schematic representation is shown in Fig. 7.

Chemical vapor deposition

Chemical vapor deposition (CVD) is a multidirectional conformal deposition technique in which a substrate surface is coated with the desired nanomaterial. The deposition is facilitated by a heat treatment followed by a chemical reaction with precursor gases. The sequence of steps is as follows: (1) reactant advent inside the reactor; (2) reaction of reactor gas; (3) diffusion of the reactant gas on substrate surface; (4) adsorption of the gaseous molecules on substrate surface; (5) surface reaction; finally, (6) by-product desorption and removal. Material of construction of substrate, reactant gas applied, and temperature and pressure exerted in the reactor chamber are essential factors on which the CVD process depends. The temperature and reaction time are crucial that influences the product formation. For example in a study involving MWCNT formation in the range of 590 and 850 °C, it was found that the higher temperature disrupted the alignment of the nanotubes. The diameter of the tubes increased from 16 nm to 45 nm with increment in temperature. Furthermore, increasing the reaction time resulted in longer tube formation [127]. The CVD can be further classified depending upon energy source, substrate, pressure, etc. as rapid thermal, laser-induced, plasma-enhanced, non-porous, atmospheric pressure, ultrahigh vacuum, direct liquid ejection, and many more. The major drawback of this method is its high cost and unsuitability for fabricating certain materials. It is widely employed technique for CNT, CNF synthesis, and synthesis of metal oxides posing specified morphology. These include granular, broccoli-like, crystallite facetted texture, semi-hexagonal shape, high crystallinity and hexagonal structure, triangles, etc. [128–132].

Apart from the above-mentioned CVD, aerosol assisted is recently developed technique and gains attention owing to its low atmospheric pressure operation [133]. It is an easily scalable single-step technique in which the solution containing the substrate is atomised and transported with the help of a carrier gas in the deposition chamber [134]. It finds applications in synthesizing photocatalysts with mixed phase deposition. In one such typical synthesis with SnO_2/TiO_2, the surface morphology changed from cassiterite SnO_2 to anatase TiO_2, while synthesizing ZrO_2/TiO_2 results in dense array of facets [133, 134]. Similar synthesis for a pure SnO_2 resulted in flattened and uniform morphology possessing round-shaped crystals and flattened grains [135].

Fig. 7 Schematic representation of various synthesis methods. **a** Arc discharge (the figure is adopted and reproduced with permission from Ref. [269]). **b** Sonochemical (the figure is adopted and reproduced with permission from Ref. [270]). **c** Exfoliation (the figure is adopted and reproduced with permission from Ref. [271]). **d** Hydrothermal (the figure is adopted and reproduced with permission from Ref. [272]). **e** Solvothermal (the figure is adopted and reproduced with permission from Ref. [273]). **f** Microwave-assisted synthesis (the figure is adopted and reproduced with permission from Ref. [274]). **g** Polyol synthesis (the figure is adopted and reproduced with permission from Ref. [275]). **h** Chemical vapor deposition (the figure is adopted and reproduced with permission from Ref. [276]). **i** Ball milling (the figure is adopted and reproduced with permission from Ref. [177]). **j** Flame spray pyrolysis (the figure is adopted and reproduced with permission from Ref. [277]). **k** Microemulsion (the figure is adopted and reproduced with permission from Ref. [278]). **l** Sol–gel method (the figure is adopted and reproduced with permission from Ref. [279]). **m** Electrodeposition (the figure is adopted and reproduced with permission from Ref. [280])

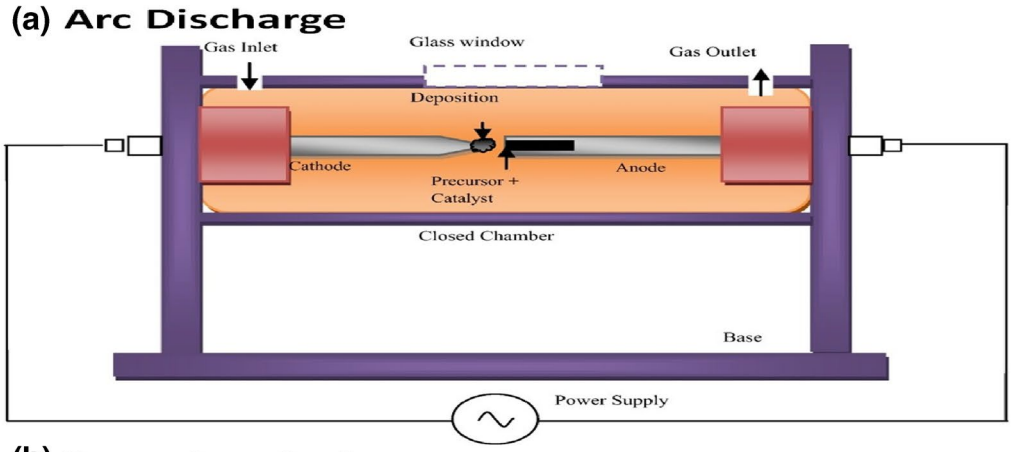
(a) Arc Discharge
Gas Inlet
Glass window
Gas Outlet
Deposition
Cathode
Precursor + Catalyst
Anode
Closed Chamber
Base
Power Supply

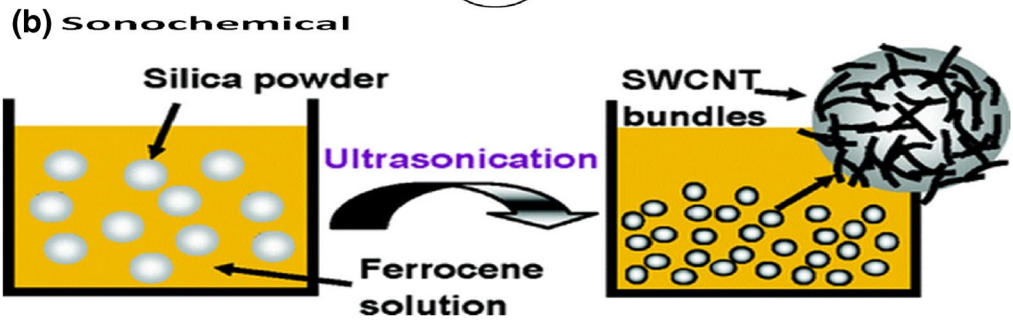
(b) Sonochemical
Silica powder
Ultrasonication
Ferrocene solution
SWCNT bundles

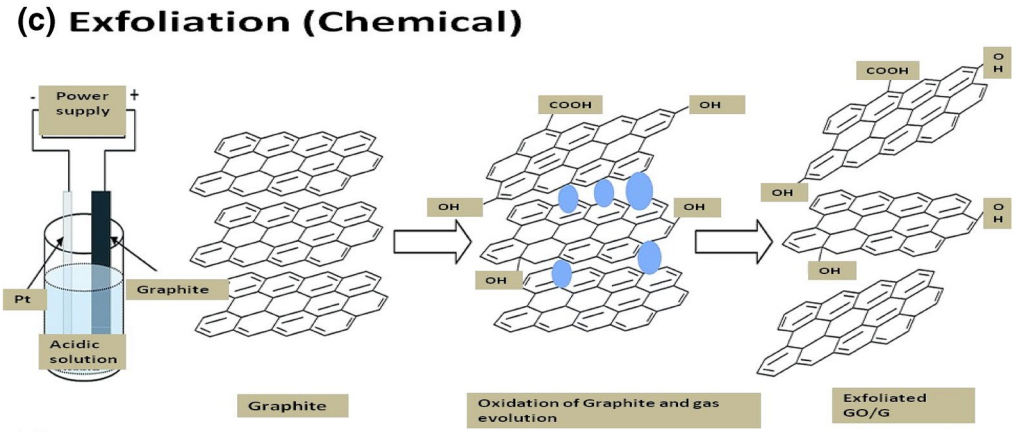
(c) Exfoliation (Chemical)
Power supply
Pt
Graphite
Acidic solution
COOH
OH
Graphite
Oxidation of Graphite and gas evolution
Exfoliated GO/G

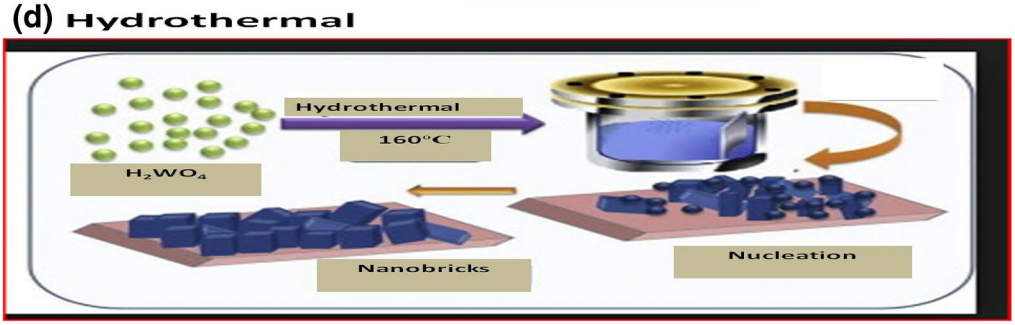
(d) Hydrothermal
Hydrothermal
160°C
H_2WO_4
Nanobricks
Nucleation

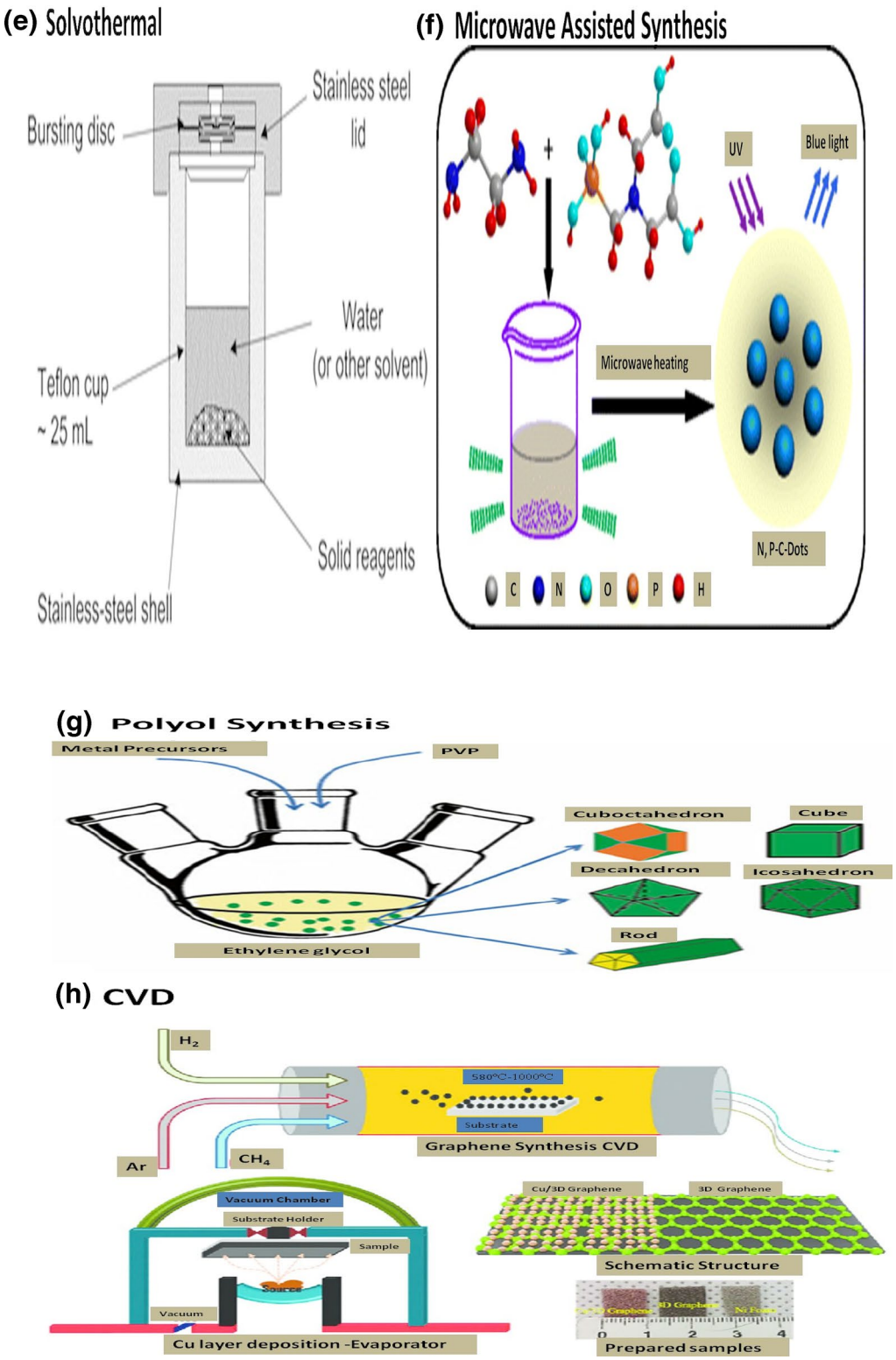

Fig. 7 (continued)

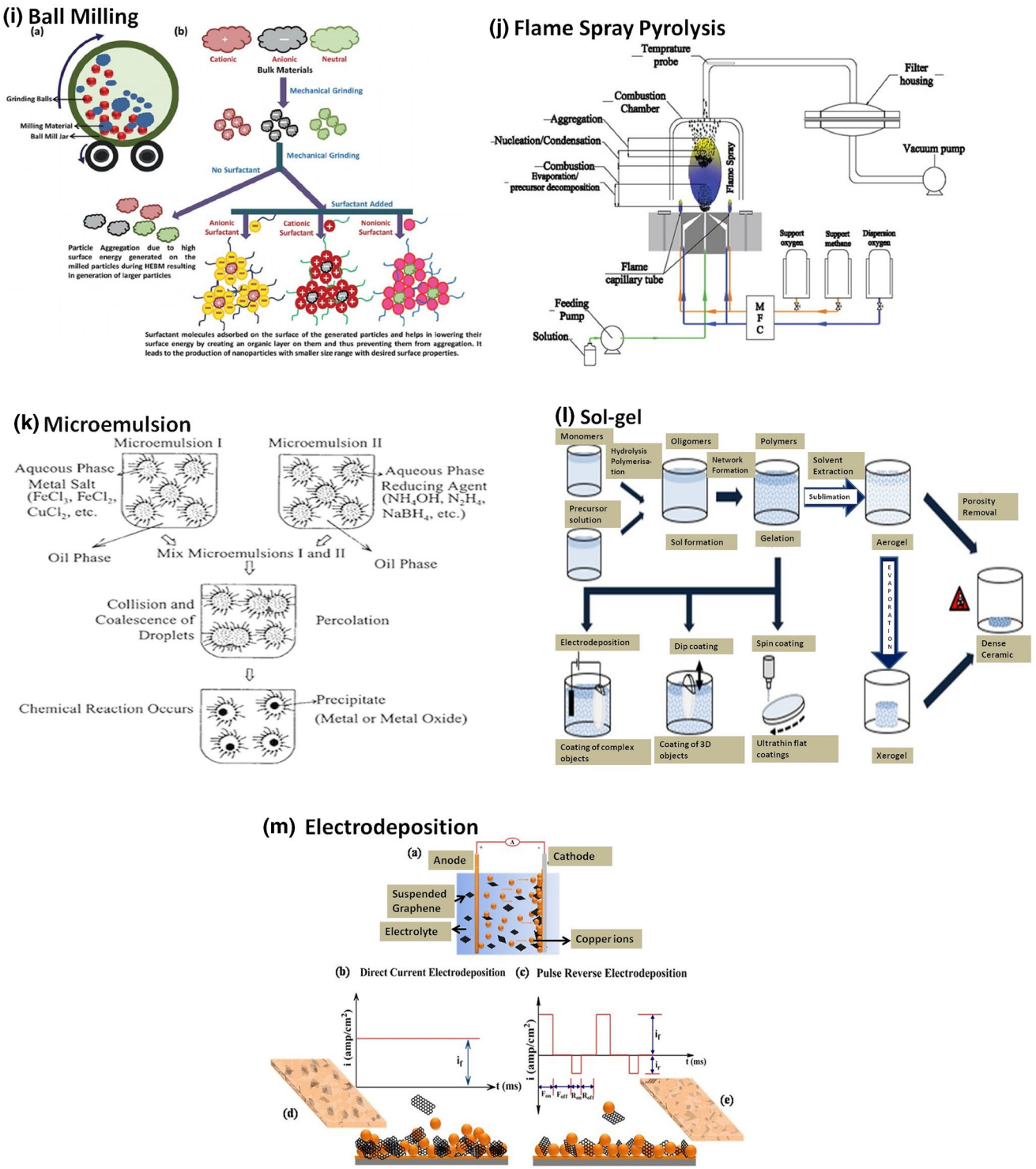

Fig. 7 (continued)

Sol–gel

Sol–gel is one among the synthesis methods that can yield high-purity nanomaterials at room temperature. It adopts colloidal with transitional solution and gel-phase formation. In general, metal alkoxides are used as precursors and these precursors serve as monomers for polymerisation which is followed by hydrolysis, condensation, and crosslinking to yield the desired gel. It is widely used flexible technique to form ceramics and composite materials with high surface

area. Its limitation includes the use of costly precursors and development of unwanted cracks on drying. pH and temperature are the factors upon which the sol–gel process depends; for instance, in PbO–TiO_2 formation, lower temperature (~ 30 °C) and acidic pH resulted in anatase structured TiO_2, while incremental (~ 70 °C, Alkaline) resulted in tetragonal structure of $PbTiO_3$ [136]. Materials like spherical-shaped C-TiO_2, 3D ordered macroporous 3DOM PW_{11}Co–APS–TiO_2 with interconnected honeycomb pore structure, spherical crystal ZnO, shapeless Fe_2O_3-TiO_2, metal ion-doped TiO_2, irregular Bi_2WO_6Porphyrin/SiO_2/Cp*Rh(bpy)Cl Hybrid to mimic chloroplast, etc. [137–143].

Pyrolysis

Pyrolysis is a vapor phase synthesis technique occurring at high temperature. It is further classified as follows:

Flame spray pyrolysis

A high-energy flame is produced in this technique using a laser employing carbon dioxide in a closed chamber. The precursors are first passed into the reaction chamber in the form of aerosol where they undergo flame treatment followed by rapid cooling to achieve the desired product. Thus, temperature is only the governing factor that can influence this technique. This can be substantiated by the $BiVO_4$ synthesis, where, at relatively low temperature, scheelite-monoclinic phase was observed, while, at higher temperature, the phase changed to tetragonal [144]. It is generally used for synthesizing crystal-modified CuS, classical non-metal-doped photocatalysts, and heterojunction composite with higher surface area [145–148].

Laser pyrolysis

It is a technique in which the substrates are decomposed in an anaerobic environment using infrared laser source. Aerosol precursor formation occurs when the reactant molecules are dissolved in a solvent followed by ultrasonic spraying. These aerosols are subjected to laser treatment resulting in final desired product [149]. The nanomaterial possesses small diameter without any agglomeration of particles [150]. Nanomaterials formed by this method include spherical-shaped N-doped and Au-loaded TiO_2 arranged in chain geometry and partially facetted TiO_2/SnO_2 [151, 152].

Hydrothermal

The hydrothermal technique employs autoclave for heating the precursors in water solvent at elevated temperature and pressure. In general, the temperature used for heating is above 100 °C and less than 300 °C. This high temperature of the closed system generates high-pressure environment aiding solubility of reactants. This hydrothermal method is a crystallisation process that involves nucleation and crystal growth as predominant steps. Due to its ease and simple operation, this method is most widely used for various nanomaterial preparations. Since temperature is the only direct controlling parameter, it has a significant influence on the product. For example, in a typical ZnO nanorod synthesis, dimensions of the nanorods were directly proportional to the temperature [153]. Moreover, the residence time could also play an effective role, as the nanorod diameter increases with increase in reaction time [153]. In the same study, pH also influenced the ZnO synthesis by changing its structural morphology, i.e., acidic pH favored nanorod morphology, whereas alkaline favored flower-like structure [153]. A variety of nanomaterials were produced by this method including heterostructures like g-C_3N_4/Bi_2WO_6 [154]. The obtained g-C_3N_4 showed aggregated laminar structure, while Bi_2WO_6 exhibited flake-like morphology. Similarly, photocatalyst possessing irregular sheet morphology, irregular particles, flower-like spheres, spherical-shaped nanoparticles, and hexagonal morphology was also synthesized by this method [155–159].

Solvothermal

The solvothermal method is similar to the hydrothermal method; only difference is that the solvent used in this technique is non-aqueous. This process depends on factors like solvent, temperature, and pressure. Organic solvents like 1, 4-butanediol produce thermally stable nanomaterials as compared to toluene [160]. In some instance, increase in temperature directly influenced the synthesis by significantly decreasing the particle size of the nanomaterial [161]. This method can be considered if the researchers are looking for a photocatalyst with defined morphology as listed: Gd-doped TiO_2 bearing hollow flower morphology, hierarchical TiO_2 of chrysanthemum flower morphology, Bi_2WO_6 with flower morphology, and many more [162–166]. In recent years, microwave-assisted solvothermal synthesis method has gained attention and deployed for synthesizing materials with more uniform structure with tunable intrinsic properties. This is due to uniform and even temperature induced by the microwave throughout the reaction [167, 168]. Few cases include synthesis of α-Fe_2O_3 nanosheet consisting of uniform hierarchical hollow mesoporous with microspheres structure and $Bi_4O_5I_2$ having uniform microsphere geometry [167, 168].

Microwave-assisted synthesis

This method employs microwave for heating of reaction mixture to synthesize nanomaterial. The rapid attainment

of high temperature and pressure by microwave heating enhances the reaction rate and homogeneous mixing. It has also made remarkable use in combination with other synthesis methods like solvothermal, sol–gel, CVD, polyol synthesis, etc. The faster reaction product with a better yield by implementing microwave with other techniques is the key factor for its application. Some of the nanomaterials obtained by synergistic effect of this method are Ag/g-C_3N_4 having crystalline Ag nanoparticle and CdS having smaller particles with enhanced monodispersity, etc. [169, 170].

Sonochemical

In sonochemical synthesis method for nanomaterials, an indirect interaction between the precursor and ultrasound via "acoustic cavitation" takes place. In this process, the ultrasound wave leads to the formation of bubbles in the sample which oscillate with collecting ultrasonic energy and grew in size. The excessive growth in size ultimately leads to its implosive collapsing leading to the release of stored energy which promotes the formation of nanomaterials. It is a preferred technique as the reaction takes place at ambient temperature. The pH is the major factor that affects the nanomaterials formed in sonochemical synthesis. When $BiPO_4$ is prepared at very low pH (~ 1), it forms irregular cluster; upon increasing (~ 5) results in rod-shaped structure, and at highly alkaline condition (~ 12), irregular particles were obtained [171]. The nanomaterials like N, Cl-co-doped TiO_2, Graphene-Ce-TiO_2, and Graphene-Fe-TiO_2, Ag-modified $Bi_4Ti_3O_{12}$, and rGO decorated with zinc sulphide, $SrMnO_3$, etc. are formed by sonochemical method [172–176].

Microemulsion

Microemulsion is a type of liquid-phase synthesis method in which reverse micelle serves as reaction unit. Oil in water or water in oil microemulsion depending on the surfactant used reactants collides with each other to nucleate and form the desired nanoparticle. Microemulsion is a facile and efficient synthesis technique providing control over the structure, shape, and porosity of the resulting nanomaterial [177]. The concentration of aqueous solution and reaction temperature are the major parameters that influence the product. In a particular TiO_2 synthesis, increasing the concentration of aqueous solution increased the particle size of the TiO_2. Moreover, by increasing the reaction temperature from 20 to 50 °C favored the increment of particle size [178]. The pH also influenced the product, as increase in pH from 8 to 10 decreased the particle size [178]. It is employed for the synthesis of a wide range of nanomaterials with defined shaped and some of them are Zn-doped TiO_2 with globular shape, BiOCl possessing hollow hemispherical shells with sheet-like structure, 2D and 3D $Bi_4O_5Br_2$, ZnO/$ZnWO_4$ heterojunction, etc. [179–182].

Arc discharge

In this technique, an arc is produced between two electrodes kept in an inert environment which leads to the deposition of nanomaterial on the electrode surface. A direct current is supplied to the electrode chamber which sublimates the anode and deposits it as nanomaterial on the cathode. The method is predominately employed for the production of fullerene and CNT. The precursors used along with its concentration are the factors upon which the product formation by arc discharge depends. A study of Wang et al. using polyvinyl alcohol (PVA) and iron as catalyst for CNT formation showed that higher PVA concentration produced entangled MWCNT with 60–190 nm diameter; however, when the concentration of iron was higher, no MWCNT formation occurred. Moreover, using PVA alone yielded MWCNT of diameter range of 30–60 nm [183]. Apart from that, it is also used in synthesizing materials like ZnO-graphene hybrid nanostructure, TiO_2/C having spherical morphology, multiwalled carbon nanotubes (MWCNTs), single-walled carbon nanohorns (SWCNHs), and multiwalled carbon nanohorns (MWCNHs) having fine well defined and straight walls, hexagonal wurtzite ZnO, and rutile TiO_2 consisting of nanorods and nanospherical structures, etc. [184–187].

Electrodeposition

Electrodeposition is a flexible, low cost, and widely used method for coating a substrate surface with nanomaterials with the aid of current. In general, it is a surface technique to improve its characteristics performed at room temperature. The electrodeposition process employs an anode and a cathode (substrate) dipped in electrolyte solution. Whenever the electricity (in the form of direct current) is passed through the electrolyte solution, the cations in the solution gets reduced and attached to the cathode surface forming a thin layer of desired nanomaterial. The thickness of the deposited nanomaterial depends on the time and intensity of current passed. Apart from them, the electrolyte temperature is a major factor influencing electrodeposition. Cu_2O thin-film formation was highly influenced by electrolyte temperature and exhibited different phase and structure at different temperature [188]. The only drawback of electrodeposition is its uneven plating thickness at the substrate surface. However, this technique can synthesize varieties of nanomaterials with specified structure and composition. Some of this includes spherical-shaped Bi_2WO_6/graphene with hierarchical structure, uniform well-aligned MnO_2/TiO_2 nanotube arrays, granular and densely agglomerated multiphase $CuInSe_2$ with spherical structure, WO_3 consisting of

irregular nanocrystalline particle, and Cu/FTO possessing hexagonal nanoslice structure [189–193].

Polyol synthesis

It is a liquid-phase synthesis method in which multivalent alcohols called polyol with precursors and capping agents are subjected to high boiling. Mostly ethylene glycol, diethylene glycol, glycerol, and butanediol are used as solvent and simple metal salts like sulphates, nitrates, halides, etc. are used as precursors. The high boiling point (200–320 °C) of polyol facilitates crystalline nanomaterial formation. The pH of the solution influences the product formed by polyol synthesis as in reduces the particle size with an increase in pH and the case was observed in Sn synthesis [194]. This method was also adopted for synthesizing materials of specified shape. Some of the reported shapes include rose flower resembled Cu_2O, highly dispersed SnO_2/TiO_2, and hierarchical spherical nanoflower-structured CuS [170, 195–198].

Exfoliation

Exfoliation is mainly used to prepare "ultrathin 2D nanomaterials". The exfoliation method can be further divided into two types.

Mechanical exfoliation

The nanomaterials are obtained by peeling of substrate surface with a scotch tape. It is a time-consuming and low yielding method, and is mostly preferred to synthesize graphene from graphite rather than any other materials.

Chemical exfoliation

The exfoliation or peel off of substrate surface takes place in chemicals. The oxidation of substrate takes place either by ultrasonication or mechanical stirring that weakens the bonding of substrate layer to yield desired nanomaterial. As like mechanical, this method is mainly employed to synthesize graphite oxide from graphite. In some instance, it is used for synthesizing photocatalyst like hexagonal SnS_2 of plate morphology, TiO_2-MoS_2 hybrid-bearing dense TiO_2 crumpled on MoS_2 nanosheet, and irregular g-C_3N_4 of tissue-like 2D nanosheet [199–201].

Ball milling

In ball milling, the samples are in powder form and are subjected to mechanical treatment for obtaining finer homogeneous nanoparticles. The sample is charged in a milling chamber-containing balls which perform the grinding operation. The chamber along with the balls is then rotated, causing collision to break the samples into smaller fragments. It is used for synthesizing selective nanomaterials and some of them are as follows: MoS_2–TiO_2 having layered MoS_2 dispersed on TiO_2, C_3N_4/TiO_2 consisting of irregularly agglomerated elliptic particles, $CoFe_2O_4$–rGO having evenly fixed $CoFe_2O_4$ nanoparticles on the stacked and wrinkled rGO sheets, CoO micropowder having nanocrystal structure, Ag/ZnO possessing aggregated crystalline structure, etc. [202–206]. High-energy ball milling is the recently preferred ball-milling technique used to synthesize several nanomaterials like $Ag/BiVO_4$, Cu_5FeS_4, etc. [207, 208].

Mechanistic features

The behavior of nanostructured material mostly depends upon the origin of material, its composites, method adopted, and various governing parameters of synthesis. The physical morphology of a particle significantly impacts the behavior of energy harnessing materials. It is a known fact that nanostructured materials possess distinct properties as compared to bulk. Equivalently, the surface characteristics also play a vital role, and moreover, the centric of the review is focused on the structure-defined mechanistic features. Over a period of years, significant efforts have been made on developing materials using various synthesis methods for achieving several morphological features. These unique features of nanostructured materials can be further tailored and engineered specifically to tackle the current challenge. The different type of nanostructures that we would be concentrating on are quantum dots, thin films, sheets, tubes, rods, fibers, wires, and various other 0-D, 1-D, and multidimensional structures. Hereon, we would discuss on the relationship between mechanistic features of the materials and the methods used for synthesis followed by its photocatalytic performance.

Zero-dimensional materials

QDs

QDs are achieved by decreasing the size of bulk semiconductor to nanometer level and the behavior of the atomic and subatomic particles impacts photon upconversion, thereby shifting the absorption towards a shorter wavelength. In a study by Zhao et al., higher charge separation leading to extended lifetime of photoinduced charges and lower recombination rate was obtained by depositing MoS_2 quantum dots on the surface of TiO_2 nanotubes. This achievement is attributed to quantum confinement effect [209]. In a similar study, CdSe quantum dot over WS_2 composite prepared by Hao and team showed efficient separation of electron hole pairs, thereby decreasing photoluminescence and enhancing

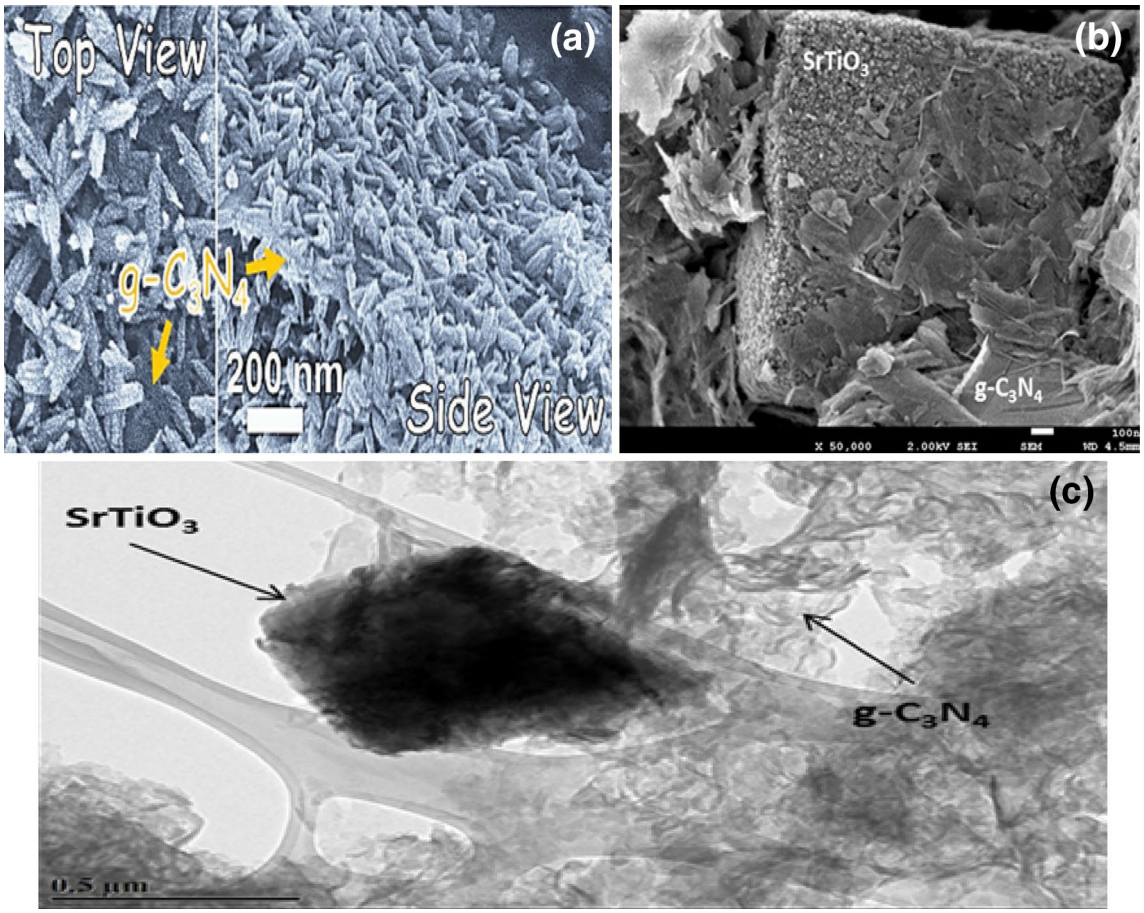

Fig. 8 SEM image of **a** $W_{18}O_{49}$/g-C_3N_4, **b** g-C_3N_4/$SrTiO_3$, and **c** HRTEM image of g-C_3N_4/$SrTiO_3$ (the figure is adopted and reproduced with permission from Refs. [213, 214]

photocatalytic performance [210]. Thus, the synergism of all these properties makes it an efficient material for light-driven applications. Although quantum dots are very attractive dimensionless material, it has drawbacks such as cytotoxicity, poor photostability, and material recovery, and hence, further research is required before it is considered for real-world applications [211].

Thin films

One of the most common and easy ways of synthesizing nanostructured materials is thin films coated on various substrates. Nanosheets and nanomembranes have similar structure as like thin films but without the support of a substrate. Dimensionally, such materials can be classified as 2-D, but most of their light-driven mechanism takes place in the third nanodimension, classifying it as a 0-D material. Light-driven application of thin films were first investigated by Fujishima's group in the early 1990s, wherein TiO_2 thin films were prepared over a silica substrate sintered at 450 °C yielding exceptional photocatalytic property as compared to classical P-25Degussa [212].

CVD and electrodeposition are the most popular and well-practised techniques for depositing desirable materials onto a substrate [128, 129, 131, 133–135, 192]. On the other hand, mechanical or chemical exfoliation can deliver photoefficient materials in the form of plate and sheet geometry [199–201]. Thin films provide excellent support systems for introducing various micro- and nanostructures onto the planar films and membranes. For example, as shown in Fig. 8(a), Zhang et al. grew rod-shaped grass-resembling monoclinic $W_{18}O_{49}$ through solvothermal route and bundled it onto g-C_3N_4 sheets by exfoliation through sonication. The obtained defined structures of the composite exhibited heterojunction through Z-scheme mechanism, resulting in enhanced visible light photocatalytic activity [213]. In similar work as shown in Fig. 8b, c, Leong and co-workers wrapped the classical perovskite ($SrTiO_3$) onto amorphous g-C_3N_4 nanosheets by a facile thermal method giving symbiotic interaction resulting in enhanced solar photocatalytic behavior [214]. Likewise, BiOBr@graphene oxide was

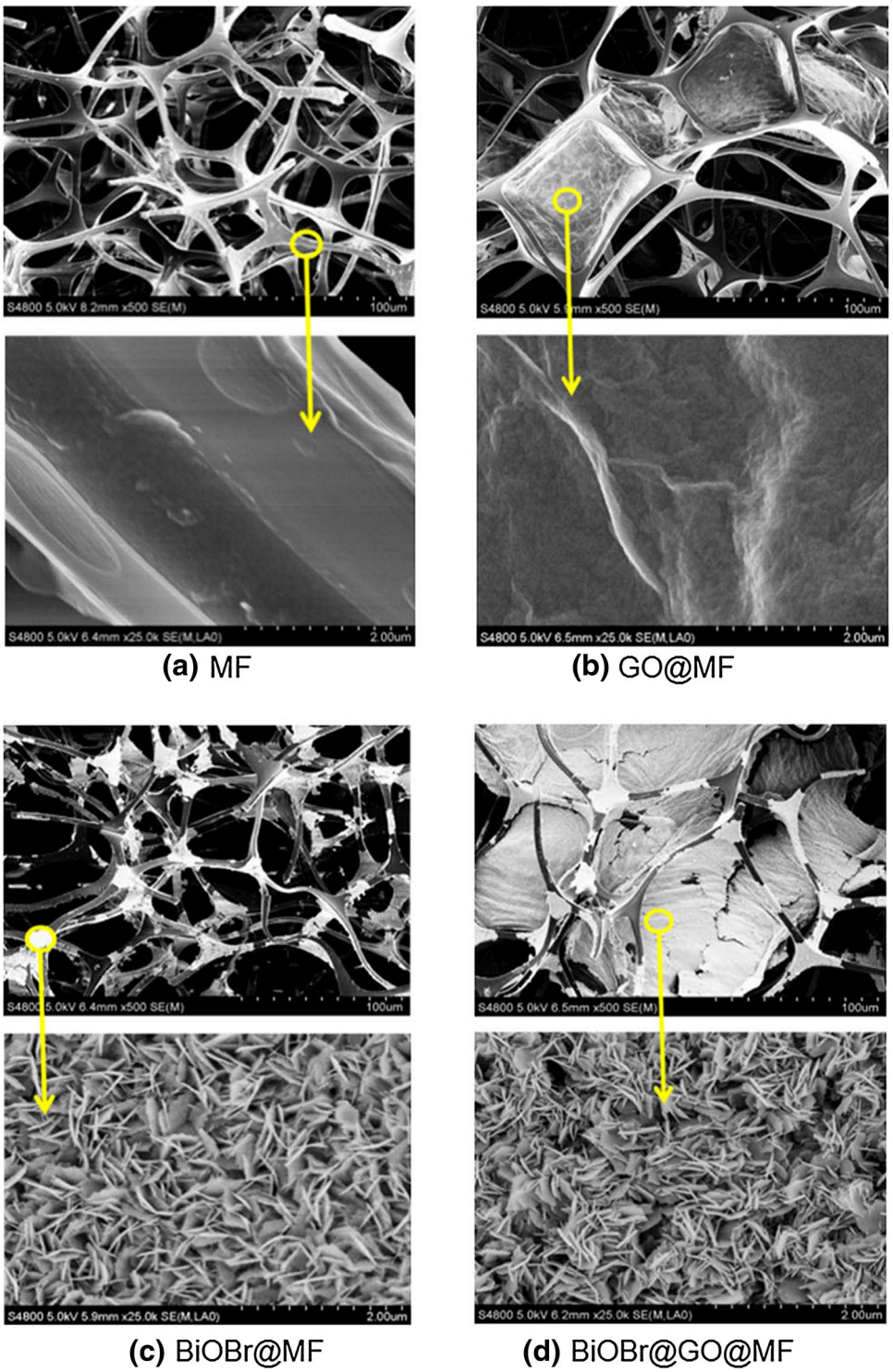

Fig. 9 SEM images of different samples of melamine foam (the figure is adopted and reproduced with permission from Ref. [215])

synthesized through solvothermal approach and wrapped around melamine foam by Huo et al.. The final ternary ends up with a structure, wherein the pollutants are transferred through channels provided by the melamine foam leading to enhanced mass transfer and visible light photocatalysis [215]. The schematics of the above-discussed materials morphologies are presented in Fig. 9.

To further enhance the photocatalytic activity of a desired material, doping of transition metals is widely practised and provides synergetic change in behavior of excitons. The controlled composition of precursors makes it easy to dope metals or elements during synthesis. Imani et al., adopted sol–gel approach for doping Cr into titania thin films forming cubic, hexagonal, and worm-like

morphologies due to varied dopant concentration. The Cr doping increased the lattice mismatch, resulting in microstructural coarsening [216]. Sayikan and team approached hydrothermally to synthesize Sn-doped TiO_2 nanoparticles and further developed a thin film by spin coating. As a result, the doped material showed a better photocatalytic degradation than that of undoped TiO_2 [217]. The use of non-metals is also practised for doping various semiconductors to improve the efficiency of energy materials [146, 147, 172]. This is achieved through a more favorable flame and laser pyrolysis route [146, 147, 151]. Using this technique, Smirniotis's team synthesized N-doped and S-doped TiO_2 thin films, while a team led by Ahmad prepared C- and S-doped and mixture of C- and S-doped TiO_2 thin films via the traditional sol–gel technique [146, 147, 218]. Ultimately, all the developed doped materials exhibited good visible light photocatalytic activity.

The above-discussed zero-dimension nanostructures owing to its unique properties obtained from quantum confinement effect have demonstrated appreciable photocatalytic activity. Furthermore, the appreciation should also be attributed to high surface area with uniform pore size distribution, thereby effectively moving the activated electron–hole pairs to the surface consequently increasing the availability of active sites for reaction.

One-dimensional materials

The basic category of one-dimensional semiconductor comprises of solid nanostructures that grow in a single direction and some classical examples are wires, rods, and simple 1-D hollow tubes. These structures have their own set of unique properties which are further reviewed and discussed in Table 1. Therefore, just by introducing various structures with unique properties has improved the photocatalytic activities of semiconductors. A schematic illustrating synthesis of 1-D nanotube arrays utilizing multiple light reflection phenomena is presented in Fig. 10 [219].

Multidimensional hierarchical hybrid materials

The advancement in the development of sophisticated instruments significantly improved and modified the synthesis approach. As a result, fabrications of multidimensional hierarchical structures were realistic. These multidimensional structured materials were economically obtained with the support of hydrothermal, solvothermal, and sol–gel methods. Such multidimensional semiconductor nanomaterials usually bear composite structures, which further tends to improve the surface area and other photocatalysis governing intrinsic properties. Recently, the focus has shifted on the formation of multidimensional semiconductors with hierarchical structures for the purpose. The most significant among those were presented in Table 2 with their salient features.

It is evident that, in most cases, the surface chemistry of a concentric core shell structure is restricted to the outer shell only, thereby urging the need to introduce a new-generation hybrid structure of non-centrosymmetric nature. The pictorial representation of such non-centrosymmetric nanostructures as described by Weng et al. is presented in Fig. 11 [220].

It is clear from the figure that the structure holds series of multiple functional units where each subunit is independently capable of functionalisation, leading to its synergisation, resulting in commanding photocatalytic activities. Although a rudimentary study was conducted by Weng et al., a further detailed investigation is required to understand its complete mechanism [220].

Noble metal deposition

Noble metal deposition onto desired metal surface is a common approach practised over decades. This is generally achieved by chemical and photo reduction or by direct deposition of chosen noble metal on to desired material [221, 222]. Interfacial contact between support and noble metal is one among the important factors on which the photocatalytic activity depends. Hence, for better interfacial contact, researchers used a direct defect-mediated growth for depositing noble metal [222]. On the other hand, the size of noble metals also has a significant effect on light-harvesting activities. This was very well revealed by a team led by Kamat, where they demonstrated the intrinsic inherent feature, i.e., shift in Fermi energy level attained by varying the Au size onto TiO_2. A greater shift in Fermi energy level was observed in smaller Au particles than the larger one. The study also showed the influence of the same on the recombination of the charge carriers, concluding the contribution of Au for visible light shift in TiO_2 and improved quantum efficiency [223].

In most cases, silver is opted by the researchers owing to its cost and delivery of better mechanistic features for light harvesting. However, a detrimental report was observed by Barakat and co-workers in which they utilised TiO_2 as a desired semiconductor. This unusual contradiction was attributed to the change in structure from fibers to rods with an increase in the silver content and the same was revealed by the team [224]. Ma and team embedded Pt on molybdenum carbide through an in situ route. This embedment allowed for better interface properties, thereby enhancing the photocatalytic activity of molybdenum carbide [225]. Though many such reports were available in the scientific database most of them were critically reviewed and reported elsewhere [226].

Table 1 Morphological and intrinsic properties of one-dimensional nanostructured materials

Material	Shape	Synthesis technique	Mechanistic feature	Unique properties	Refs.
TiO_2	Nanotube	Electrochemical method	Length and inner diameter of the nanotube increased linearly with increasing anodization voltages	Red shift in absorption wavelength due to confinement effect of nanodimensioned nanotube wall	[281]
Pd/TiO_2, Pd/CeO_2, Pd/WO_3	Nanotube, nanofiber, nanoparticles	Sol–gel and hydrothermal method	The various synthesis methods used gave different unique structures	Even though nanofibres had less surface area, the high photocatalytic activity was due to the interaction between nanofibres and Pd nanoparticles	[282]
Bi_2MoO_6	Nanosheets, microrods	Hydrothermal method	Various morphologies were obtained by varying the pH in precursor solution	Although microrods had a better crystallinity, the increase in photo activity of nanosheets was proved to be due to change in morphological structure	[283]
$BiVO_4$	Ax gourd, needle-like structure	Hydrothermal method	Various morphologies were obtained by varying the pH in precursor solution	The needle-like structure allows for higher surface area and faster electron transfer. Monoclinic crystal structure gives a better photocatalytic efficiency than tetragonal crystal structure due to overlap of Bi 6s and O 2p orbitals	[284, 285]
ZrO_2	Nanoparticles	Pyrolysis	Change in synthesis temperature gave different crystal structures	Monoclinic crystal structure showed a better photocatalytic activity than tetragonal crystal structure	[286]
WO_3	Nanowires, nanoparticles	Thermal annealing	Change in synthesis temperature gave different crystal structures	Monoclinic crystal structure is more photoefficient than hexagonal crystal structure. Nanowires show higher efficiency than nanoparticles owing to their higher surface area and better charge carrier ability	[287]
$rGO/Pt\text{-}TiO_2$	Nanotube arrays	Photo deposition, thermal reduction	Pt nanoparticles are uniformly dispersed onto the canopy and inner walls of titanium nanotubes	Pt deposition onto inner walls shows higher photocatalytic activity due to higher synergism between Pt and TiO_2	[219]
TiO_2	Nanotubes	Hydrothermal method	The synthesis method and precursors were chosen, as to give a hollow structure	Laser flash photolysis showed that the half-life of the photogenerated holes was longer for titania nanotubes compared to that of nanoparticle structures, which can be attributed to the hollow structure	[288]

Table 1 (continued)

Material	Shape	Synthesis technique	Mechanistic feature	Unique properties	Refs.
Fe_2O_3/TiO_2	Microrods, microtubes and nanorods	Co-precipitation and wet chemical method	Change in precursor from Fe(II)-oxalato to Fe(II)/Fe(III)-oxalato which resulted in change from microrod to microtube	The photocatalytic degradation efficiency increases as the morphology changes from microrods to microtubes to nanorods due to higher number of available active site	[289]
ZnO–ZnS	Nanorods with ZnS shell layers	Hydrothermal sulfidation reaction	ZnS shell layers gave a granular structure to the ZnO–ZnS composite rods	The granular structure and higher crystallinity along with increase in the formation of defects in ZnS shell layers are the reasons for the improved light-harvesting ability	[46]
Ag_2CrO_4	Porous nanoparticles	Microemulsion, precipitation, hydrothermal	Micro- emulsion synthesis gave a more homogeneous structure	Defect free homogeneous morphological structure has shown to have higher photocatalytic activity	[290]
Defect-induced ZnO	Nanorods	Atomic layer deposition, rapid thermal annealing	Defects were intentionally introduced using different synthesis methods	Defects are present on the edges, thus giving a better electron transfer and light trapping sites, leading to improved dye degradation	[291]

Application of nanostructured materials

In energy conservation and generation, photocatalysis can aid in two particular ways: (1) water splitting reactions for H_2 production and (2) direct photoreduction of CO_2. Photocatalysis in a sequence can be described as follows. The first step in photocatalysis involves absorption of suitable wavelength of solar energy, such that its energy exceeds the band-gap energy. In the second step, thus, the photo-excited electron moves from valence band to conduction band forming an electron–hole pair favoring redox reaction at the valence and conduction band. Hence, an effective photocatalyst is one which possesses low band-gap energy, resisting ability to prevent recombination of electron–hole pairs, and high redox potential. This section discusses various operation parameters, its interplay with the performance, some challenges and strategies adopted in the application of nanostructured materials in energy, environmental safety, and remediation. Table 3 presents various photocatalysts that have been used for water splitting reaction, CO_2 photoreduction and degradation pesticides, and other persistent organic pollutants (POPs). This section emphasizes on the modifications that have been performed for the light-driven energy applications.

Water split application of the nanostructure photocatalyst

Titanium oxide is one of the most widely studied photocatalysts as it has low toxicity, high chemical and biological inertness, and high photocatalytic reactivity [227]. Its limitation is that it is naturally activated by UV radiations which form a very low percent of solar spectrum [228]. However, doping with transitional metals such as Pt, V, Cr, or Fe have enabled the absorption spectrum towards visible. In a similar effort, hierarchal porous structure (HPT-500) TiO_2 was deposited with Pt and Zinc phthalocyanine (PCH-001) to form a composite. The results showed that Pt-HPT nanocomposite with 0.25 µmol/15 mg of nanocomposite (HPT-0.25) exhibited maximum H_2 evolution. The H_2 yield was found to be 2260 µmol at $\lambda \geq 450$ nm (300 W xenon arc lamp) and the turn over number was found to be 18,080. Highest apparent quantum yield (AQY) of 11.97% was achieved at 690 nm for HPT-0.25 [229].

Exfoliation is a technique that can either modify or reduce the size of the photocatalysts. One major advantage of using exfoliation is that it does not alter the crystal structure. Due to reduction in size, the migration distance of charge carriers is reduced and the surface area of the catalyst is increased [230]. In spite of this, one challenge faced in the exfoliation is excessive time consumption and low-scale production. To address this issue, Yuchao and Liejin engineered a

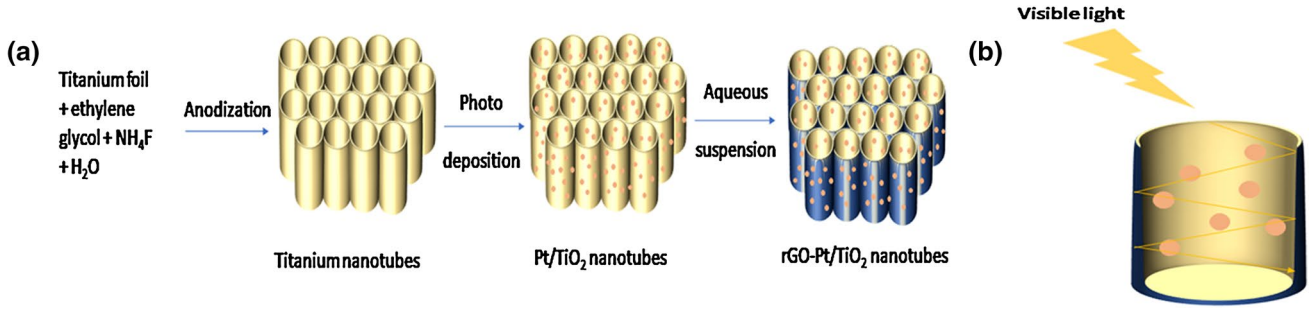

Fig. 10 Formation mechanism of rGO-Pt/TiO_2 nanotubes (**a**) and multiple light reflections in rGO-Pt/TiO_2 nanotube structure (**b**)

new ultrasonic method for rapid and high yield of (TBA/H) $Pb_2Nb_3O_{10}$ by exfoliation. The obtained (TBA/H)$Pb_2Nb_3O_{10}$ was loaded with Pt and used as visible light photocatalyst for production of hydrogen ($\lambda > 415$ nm), thereby making it as a first and foremost visible light-driven $AB_2Nb_3O_{10}$. The perovskite yielded 50 mmol/h and 17 mmol/h of H_2 under full-arc and visible light irradiation, respectively. The study concluded that, due to smaller migration distance of charge carriers, efficiency of electrons for hydrogen production improved [231]. Perovskite nanosheets can also improve the photocatalytic activity. In one such study, experiment with $HCa_2Nb_2TaO_{10}$ was performed. This particular perovskite displayed a quantum yield of 80% at 300 nm for H_2 evolution. This study concluded that the composition of metal oxides played a key role in determining the photocatalytic activity [232].

CQDs along with graphene QDs have become very popular in photocatalytic energy applications. The desired feature of the CQDs is broad optical absorption accounting for photoluminescence [233, 234]. In addition, the optical absorption is in the range of UV–Vis and up to near IR [235]. Hence, the core carbon nanoparticle can use the visible light to generate necessary charge carriers for catalytic energy conversion. Similar property is also exhibited by graphene QDs and other carbon-based QDs [236]. However, in present scenario, many reported catalysts suffer low quantum efficiency with solar-to-hydrogen (STH) ratio less than 0.1%, high cost, and poor stability [237]. To combat this issue, Carbon nanodot-carbon nitride (C_3N_4) has been reported with high performance for water splitting reactions using solar energy. Carbon nitride is found in high quantity on the earth crust, and thus, it lowers the cost of production. This composite exhibited a decreased bandgap of 2.77 eV with increased visible light absorption and quantum efficiency of 16%. The overall solar energy conversion efficiency was reported to be 2.0% [238].

Shinde et al. reported improvement in photocatalytic activity of g-C_3N_4 under visible light irradiation by doping it with carbon dots and TiN nanoparticles. The prepared composite showed sixfold increases in photocatalytic activity as compared to pure g-C_3N_4. Doping with carbon dots eliminated the problem of C_3N_4 poisoning by H_2O_2 [238]. Utilizing the broadband plasmonic resonance of TiN nanoparticles increased the absorption spectrum from UV–Vis to NIR (320–700 nm), thereby convalescing the performance of photoelectrochemical water splitting. The calculated incident photon-to-current efficiency for pure C_3N_4 was found to be in the range of 0.089–0.00077% and that for TiN-C_3N_4-C dots was 1.143 to 0.0056% for 400–700 nm [239].

Graphene has some distinct properties like high work function, intrinsic electron mobility, and optical transmittance which make it highly suitable for photocatalytic activity [240]. Thus, it rapidly accepts, transfers electrons, and decreases the recombination rate. Graphene has been used as a co-catalyst in a study by Mateo et al., where a few layers of graphene were used to support Cu_2O nanoplates bearing 2.0.0 facet. The prepared Cu_2O strongly interacted with graphene and improved hydrogen yield to 19.5 mmol/g in the presence of 300 W Xe lamp [241].

Nanostructure photocatalyst for driving artificial photosynthesis

Photocatalytic conversion of carbon dioxide into methane (fuel) has been considered as an efficient and viable technique for dealing with the global environment challenge of carbon sequestration. TiO_2 and CdS are popular semiconductor nanomaterials employed for this purpose; however, the problem with most is that they get excited only in the UV region [242]. Lin et al. created a photosystem with g-C_3N_4 as a photocatalyst with triethanolamine (TEOA) as hydrogen and electron source. Here, Co^{2+} ion when coordinated with bipyridine ligand activated the electron transfer process. g-C_3N_4 was coated with cobalt oxides (oxidative catalyst) which aided in transfer of light generated electron–hole pair with a turnover number of 4.3. The reduction of CO_2 resulted in 3.7 µmol of CO and 0.6 µmol of H_2. It was also noted that low Co^{2+} concentration was beneficial

Table 2 Morphological and intrinsic properties of multidimensional nanostructure materials

Material	Shape	Synthesis technique	Mechanistic features	Unique properties	Refs.
C_{60}/g-C_3N_4 using DFT	Wrinkle type, flat	–	A significant change in morphology, from flat to wrinkle type due to adsorption of C_{60} onto g-C_3N_4 monolayer	Wrinkled structure augments the light absorption giving improved photocatalytic performance and a stronger photooxidation capability when compared to flat structure as the valence band maximum shifts towards a lower position	[292]
$CuInSe_2$	Nanoslices, nanodendrites	Pulsed electrodeposition	By tailoring pulse shape and duration, this technique enables close control of the nucleation and growth processes and allows modification of film nanostructure	The nanodendrites show lower recombination rates owing to its structure	[193]
BiOBr	Crisscrossed nanosheets	Hydrothermal followed by solvothermal	The [C16 min] + IL is essential for the horizontal assembly rather than gathering of BiOBr nanosheets, giving crisscrossed structure	Crisscross textured BiOBr nanosheets enhanced light absorption due to the multiscattering of light occurring in its internal surface	[293]
$CdIn_2S_4$	Yolk shell of varying sizes, hollow and solid spheres	Hydrothermal	Different structures were obtained by varying the synthesis reaction time	Multiple reflections was favored due to presence of certain hollow inner microspheres in the yolk shell structure, thus allowing greater amount of light to absorbed	[294]
CuS	Nanoflowers, nanoplates	Polyol	CuS spherical nanoflowers composed with multilayered nanoplates produced With a medium releasing rate of S^2, while at the other releasing rates monodispersed hexagonal nanoplates or disordered nanoplate complexes resulted	The hierarchical plate structure obtained had the best electrocatalytic and photocatalytic performances owing to its large surface area and multiple light reflection	[198]
TiO_2	Multichannel nanofibers	Multifluidic compound-jet electrospinning	Changes in compound jet gives a varied number of channels in nanofibers	The multichannelled hollow structure allowed for effective trapping of gaseous molecules and multiple reflections of incident light revealing a very high photocatalytic activity	[295]
Titania	Nanospheres with urchin like morphology on inner surface, sphere in sphere structure	Solvothermal technique	The inner structure changed with the change in reaction time of a solvothermal reaction	Good photocatalytic performance due to multiple reflections of light in the interior voids	[296]
Ag@TiO_2	Core shell nanoparticles	Sol–gel	The base structure was found only in solutions with low Ti:Ag mole ratio (2–6%)	Nanoparticles are encapsulated by a covering shell of noble metals and hence a better interfacial contact for producing a better charge carrier transport and other synergistic properties	[297]

Table 2 (continued)

Material	Shape	Synthesis technique	Mechanistic features	Unique properties	Refs.
$Pt/SiO_2/Ta_3N_5$	Core shell nanoparticles	Sol–gel	IrO_2 or CoO_x on the outer Ta_3N_5 shell surface, whereas Pt nanoparticles on the inner shell surface	IrO_2 or CoO_x acted as a hole collector, while Pt nanoparticles acted as an electron collector	[298]
$BiVO_4$/carbon-coated Cu_2O photoelectrode	Nanowire arrays (NWAs)	Electrochemical anodization followed by thermal annealing and SILAR method	CuO_2 NWAs were obtained by dehydration and oxygen removal of already available $Cu(OH)_2$ NWAs	The enhancement of photocurrent was ascribed to the efficient visible light absorption by 3-D NWAs and efficient charge carrier transfer of 1-D nanowire structure	[299]
Pt nanodot deposited $PbTiO_3$ nanotube array photoelectrode	Nanodot, nanotube array	Hard templating on a transparent conducting glass	Pt sol infiltration into the $PbTiO_3$ nanotubes	The effect of nanotube arrays and Pt infiltration on the inner side leads to augmentation of charge-carrier separation and decrease in recombination rates	[300]

for selective reduction of CO_2, whereas an increase in Co^{2+} favored the H_2 production [243].

In a recent path breaking study, strontium titanium nanorods were used as UV light-harvesting photocatalyst along with Cu_xO nanocluster and cobalt phosphate as co-catalyst to enhance the selectivity of CO_2 using water as the donor molecule. The team constructed an artificial, wireless leaf like plate using $SrTiO_3$ film deposited with Cu_xO by simple impregnation method. As a co-catalyst, cobalt and phosphate nanoparticles were later deposited on the film using photoelectrochemical method. TEM reports showed that the deposited co-catalyst was highly dispersed onto the porous structure of STO, enhancing electron–hole pairs. The result was first of its kind as it displayed 80% selectivity for CO generation over H_2 production using Hg–Xe lamp. The reported co-catalyst-loaded $SrTiO_3$ film showed 2.5 times more CO formation than bare $SrTiO_3$ film [244].

Fabrication of noble metal-free polyoxometalates (POM) reduces the cost of photocatalysts to a great extent. One such effort is seen in a study by Zhou et al. while synthesizing Co_4 doped g-C_3N_4. Modification with Co_4 increased the oxidative capacity of g-C_3N_4 and led to increased reduction of CO_2 and enabled ease charge transfer. This hybrid displayed higher yield of CO from CO_2 in the order of 107 μmol g^{-1} h^{-1} (43% wt. of CoO_4) at $\lambda \leq 420$ nm with 94% selectivity. Prolonging the irradiation up to 10 h, CO yield surged to a maximum of 896 μmol g^{-1} h^{-1} [245]. Rhenium has been widely explored for reducing CO_2 due to desirable photocatalytic properties of the former. In a study $Re_3(5\text{-dmb})^{3+}$/fac-$[Re(bpy)(CO)_3(MeCN)]^+$ was used as photocatalyst for conversion of CO_2 to CO. Trinuclear Re ring were used as a redox photosensitizer and fac-$[Re(bpy)(CO)_3(MeCN)]$ as a catalyst. The π–π interaction in the Re ring increased the lifetime of the electrons in excited state. This combination reduced the CO_2 to CO with the highest quantum yield of 82% at $\lambda = 436$ nm [246].

Wang et al. obviated the use of expensive noble metals by replacing with CuO-ZnO. Both ZnO and CuO was synthesized in the wire form where ZnO was deposited on CuO using atomic layer deposition technique. ZnO grew epitaxially, demonstrating island growth mechanism that favored recombination free transfer of electrons. The defects created by ZnO increased the life time of the electrons. The maximum CO yield under UV–visible–NIR ($250\ \text{nm} \leq \lambda \leq 810\ \text{nm}$) was 1.98 mmol g-$cat^{-1}$ h^{-1} for eight cycles of atomic layer deposition of ZnO with lower quantum yield [247]. Tungsten selenide in composite with graphene was attempted for direct CO_2 reduction. The photocatalytic efficiency was increased for WSe_2 by efficient reduction in recombination of electron–hole pairs with increase in electron transport facilitated by graphene. The study utilized an additional sacrificial agent in the form of Na_2S/Na_2SO_3. The CO_2 was reduced to methanol with a

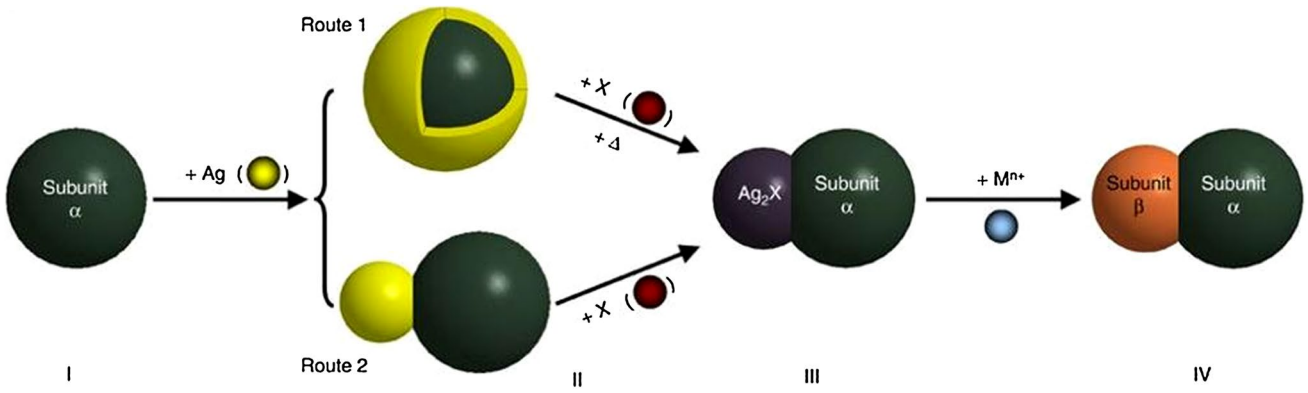

Fig. 11 Schematic showing development of non-centrosymmetric nanostructures (the figure is adopted and reproduced with permission from Ref. [220])

maximum yield of 4.3257 μmol g^{-1} h^{-1} under visible light and 5.0278 μmol g^{-1} h^{-1} under UV light [248].

Nanostructure photocatalysts for water and wastewater treatment

Nanostructured photocatalytic materials are widely used to purify both water, wastewater and they are known for degrading the recalcitrant organics. The most common materials widely used include TiO_2, ZnO, WO_3, g-C_3N_4, etc. [6–12, 249–256]. Photocatalysts have proven to be helpful in degrading several categories of organic contaminants including POPs and endocrine disrupting compounds (EDCs). Various parameters that affect the photocatalysis include pH, availability of solar light, band structure of the photocatalyst, concentration of the photocatalyst, concentration of pollutant, etc. pH of the reaction mixture exhibits profound effect on the degradation of pollutants, for instance, in an experiment performed by Yosefi and Haghighi [249], it was found that the photocatalyst heterojunction (p-BiOI/p-NiO) was able to degrade acid orange 7 more effectively at strong acidic condition as compared to neutral. The acidic condition modified the surface charge of the photocatalyst and thus enhanced the degradation process. Other important parameters that can affect the degradation process are photocatalyst dosage and pollutant concentration. Higher concentration of photocatalyst can lead to agglomeration, while pollutant can prevent sunlight from reaching the surface of photocatalyst [249].

A major challenge observed by the researchers was separation of nanoparticles after the completion of the treatment. This was overcome by decorating TiO_2 with ferromagnetic (N-TiO_2@SiO_2@Fe_3O_4), which imparts magnetic properties leading to easy separation [250]. Another approach adopted by researchers to solve this problem is immobilisation of nanoparticles. This strategy prevents the photocatalyst from washing out as well as increases its reusability. However, a major problem associated with immobilisation was the poor degradation rate of pollutant because of its decreased surface area-to-volume ratio. Furthermore, to resolve this problem, Tototzintle and group used H_2O_2 as an external electron acceptor. The usage of H_2O_2 increased the production of hydroxyl radicals, thereby enhancing the photocatalysis [251]. A usual problem faced by most researchers with metal sulphide was their instability caused by the self-oxidation of sulphide ions. The conjugation of chitosan with metal sulphide (ZnS) eliminated the self-oxidation issue where the chitosan acted as a capping ligand. [252].

Synergizing photocatalysis with processes like adsorption can show a greater impact. In a similar approach, a Fe_3O_4/$BiVO_4$ heterojunction was synergised with *Pinus roxburghii*-derived biochar and studied for the degradation of methyl paraben. It was found that the photocatalyst was able to degrade only 74.98% of methyl paraben, whereas the photocatalysis adsorption synergised was able to degrade 95.64%. The presence of biochar clearly acted as adsorbent which accumulated larger amount of methyl paraben molecules on its surface and thus allowed its easier degradation. Furthermore, the presence of Fe_3O_4 allowed easy separation of the composite after treatment [253]. Several other challenges faced by the researchers and the respective strategies chosen to solve the issue are presented in Table 3.

Future prospect

Environmental challenges and energy crisis are the biggest concern of this era; however, its solution is hidden in an outskirt domain of "nanotechnology". It refers to the exploitation of the incredible physiochemical properties of materials which have been attained by manipulating the size and structure of the material. After the discovery of light-assisted catalysis, engineered nanostructured material has become more popular tool to harvest photon energy from solar spectrum [254, 255]. Later, this technology was extended

Table 3 Nanostructure photocatalyst materials for energy and environmental application

Photocatalyst	Material description	Light source	Application	Inference	Refs.
Perovskite structure of Sr_2TiO_4 co-doped with La/N	$Sr_{2-x}La_xTiO_{4-y}N_y$ ($0 \le x \le 0.5$) was formed which shifted the light absorption range up to 650 nm. La/N doping plays binary role in increasing valence band and balancing charge inconsistency. The structure of Sr_2TiO_4 is found to be efficient in creating a smooth charge transfer pathway	300 W Xe lamp	H_2 and O_2 evolution	16 µmol/h of H_2 produced at $X = 0.3$, 13 µmol/h of O_2 produced at $X = 0.2$, at $\lambda \ge 400$ nm	[301]
$SrTiO_3$ doped with Al and Co loaded with rhodium-chromium and molybdenum oxides	Partially oxidized and reduced states of MoO_3 obtained after calcination led to enhancement of the photocatalytic activity	Xe lamp ($\lambda \ge 300$ nm)	H_2 evolution	AQY of 69% was achieved at 365 nm	[302]
Ga_2O_3 doped with Zn ion/ $Rh_{0.5}Cr_{1.5}O_3$ as co-catalyst	The calcination of Ga_2O_3 while synthesizing leads to homogenous spreading of Ca^{2+} ions on its surface. This greatly enhanced the photocatalytic efficiency. Apart from this, the semiconductor was also doped with Zn^{2+} ions and $Rh_{0.5}Cr_{1.5}O_3$ was used as a co-catalyst	450 W-Hg lamp	H_2 evolution	AQI of 71% was achieved at 254 nm	[303]
Cobalt phosphorous on a few layers of black phosphorous nanosheets	A decrease in band-gap energy was observed from 1.16 eV for black phosphorous to 1.14 eV for CoP-doped black phosphorous	Xe lamp irradiation $\lambda \ge 420$ nm	H_2 evolution	The Co–P deposited on the BP showed a H_2 evolution of 15 µmol/h, which is 12 times as compared to unaltered black phosphorous. The composite showed AQY of 42.55% at 430 nm	[304]
$rGO/InVO_4/Fe_2O_3$	A combination of $InVO_4/Fe_2O_3$ semiconductor was deposited on Chitosan Functionalized rGO surface to construct a heterostructured Z-scheme photocatalyst. The synchronised structural behavior of $rGO/InVO_4/Fe_2O_3$ led to efficient charge separation and mobility. The lower bandgap of Fe_2O_3 instantiated the Z scheme photocatalytic activity	20 W white cold LED as visible light source	$CO_{2\ to}\ CH_4$	16.9 mmol/g catalyst of methane was obtained under visible light irradiation	[305]

Table 3 (continued)

Photocatalyst	Material description	Light source	Application	Inference	Refs.
Perovskite CsPbBr QD/GO	Introduction of graphene oxide facilitated new energy transfer route. It was also able to curb the resistance in charge transfer. Ethyl acetate was used as solvent for stability of photocatalyst and increased solubility of CO_2	100 W Xe lamp with AM 1.5G filter	CO_2 to CO, CH_4, and H_2	Production of CO_2 reduction products was 57.8 µmol/g of carbon monoxide and 29.6 µmol/g of CH_4 and 1.58 µmol/g of H_2	[306]
SnS_2 – C	The doping leads to formation of well-interconnected planar structure. As a result, there is little diffusion time and quick charge transfer	Visible light irradiation	CO_2 to acetaldehyde	CO_2 was photoreduced to acetaldehyde in gas phase with a quantum efficiency of 0.7%. 125.66 µmol/100 mg.catalyst of acetaldehyde was produced. The composite displayed a high photocatalytic efficiency at 560 nm and above	[47]
N-doped TiO_2	TiO_2 doped with nitrogen, resulted in decrease in bandgap from 3.22 to 3.12 eV	Fluorescent radiation (400–700 nm)	Methyl benzene degradation	74% degradation of methyl benzene achieved	[6]
N-TiO_2@SiO_2@Fe_3O_4	TiO_2 coupled with Fe_3O_4 which imparted magnetic characters on the nanoparticle, thus resulted in its easy separation from the treated water	Compact fluorescent lamp(visible source) and light-emitting diodes	Ibuprophen, benzophenone-3(BZ-3), carbamazepine (PPCP) degradation	94% Ibuprophen removed, 93% BZ-3 removed and 71% carbamazepine removed	[250]
Cu doped Fe_2O_3	Fe_2O_3 doped with Ni, Cu, and Co	150 W tungsten lamp	Acid red 27 degradation	Photocatalytic activity of Cu-Fe_2O_3 was more than others. 98.05% degradation achieved. The photocatalyst can be reused four times	[7]
Ag_2O/GO	GO acted as supporting material on which Ag_2O nanoparticles were randomly distributed	500 W Xenon mercury lamp	Methylene blue and rhodamine B degradation	Ag_2O/GO nanocomposite resulted in improved catalytic efficiency than the pure Ag_2O particles. 97% dye removed	[8]
Fe-doped ZnS quantum dots	Quantum dots were doped with Fe^{3+} ions which resulted in blue shift in the light absorption range	40 W mercury lamp	Malachite Green degradation	99% dye degradation achieved by the doped one within 120 min at 15 mg/l dye concentration	[9]
CuO/ZnO	Formation of heterostructure between CuO and ZnO	150 W tungsten halogen lamp	Acid red 88 degradation	Twofold higher photocatalytic activity of the synthesized nanocomposite compared to bare ZnO. Addition of external electron acceptor resulted in 100% TOC removal after the total decolorization of the dye	[10]

Table 3 (continued)

Photocatalyst	Material description	Light source	Application	Inference	Refs.
Carbon dots/g-C_3N_4	Carbon dots prepared from sugarcane juice. Carbon dots acted as sensitizers on the g-C_3N_4 surface which enhanced the BPA degradation	Solar light	Bisphenol A(BPA) degradation	100% removal of BPA achieved in 90 min. Pure g-C_3N_4 was able to remove only 68.2% of BPA	[11]
TiO_2	TiO_2 pellets immobilised on rotating disk photocatalytic reactor(RDPR)	Low-pressure mercury UV tubes (four tubes, 15 W each with predominant emission of 365 nm radiation)	Chlorinated phenols and pesticides degradation	More than 80% of phenol and the phenolic derivatives removed, 63% lindane degradation	[12]

to develop more efficient nanostructured assemblies with captivating designs for enhancing surface plasmonic, since the manipulation in morphology and topography of materials can modify the intrinsic properties of nanomaterials. Therefore, architecting of nanomaterials in varying fashion to enhance the efficacy and surface plasmonic performance has piqued the global attention and becomes a fascinating approach [255, 256].

These reviewed designs and approach are attractive in the arena of nanotechnology. Yet, biomimicking is emerging as a pioneer technology to revolutionize the scientific world with a modern notion to light-assisted designs. Bioinspired duplicating of hierarchical structures demonstrates great design that instigated the distinctive architectures of biological world. A few such reports include replicate of photosynthetic pigment of cyanobacteria, scale of butterfly wings and snake, plant leaves, and spine of some marine polychaete worms [226, 257, 258]. For example, absorbance of wide range of solar light (300–800 nm) has been inferred in the wings of Paysandisia archon moth owing to the nanostructured fabrication of wing scale. The hierarchical assembling of various pigmentary nanostructures of 3D photonic crystals in the upper lamella of wing scale is finely tuned with light absorption to perform the photocoloration. A highest visible and NIR light utilisation was observed for dark black-colored spotted areas of wings, while the lowest for white-colored spots [259]. Therefore, this nanostructured fabrication of wing scale can be a good alternative to develop energy materials [260, 261]. Similarly, biomimicking of natural photosynthesis phenomenon to construct the artificial novel photosynthetic antenna is another promising green approach to maximise the harnessing of the photons [141]. The metabolic and photosynthetic activities of floral pigments of biological world were emulated for enhancing the photon utilisation and CO_2 transformation. However, in some cases, the characteristics of chlorophyll stacks were tailored for effective electron transfer [262, 263]. In a typical study, graphitic nitride nanopaper has been employed to synthesize the biomimicked photosynthetic nanostructured leaf along with zeolitic imidazolate frameworks (ZIF-9 metal organic framework) and Au stacked like thylakoids. The ZIF-9 in the composite performed electron transport and redox reaction to reduce the CO_2, while Au enhanced the light-harvesting capacity of the material. The coupling of graphene-nitride nanolayer with ZIF-9 MOF created interferences at the junctions and modified the band structure. This ternary was successfully tested for water splitting and CO_2 reduction [257]. The design and mechanistic utility of the fabricated materials is illustrated in Fig. 12 [257]. Similar mechanism of marine diatoms for mimicking the photosynthetic properties of Photosystem I (PSI) was imitated to architect the artificial diatom frustules with graphitic nitride material (C_3N_4 (DE-g-C_3N_4). Here, the reduction of

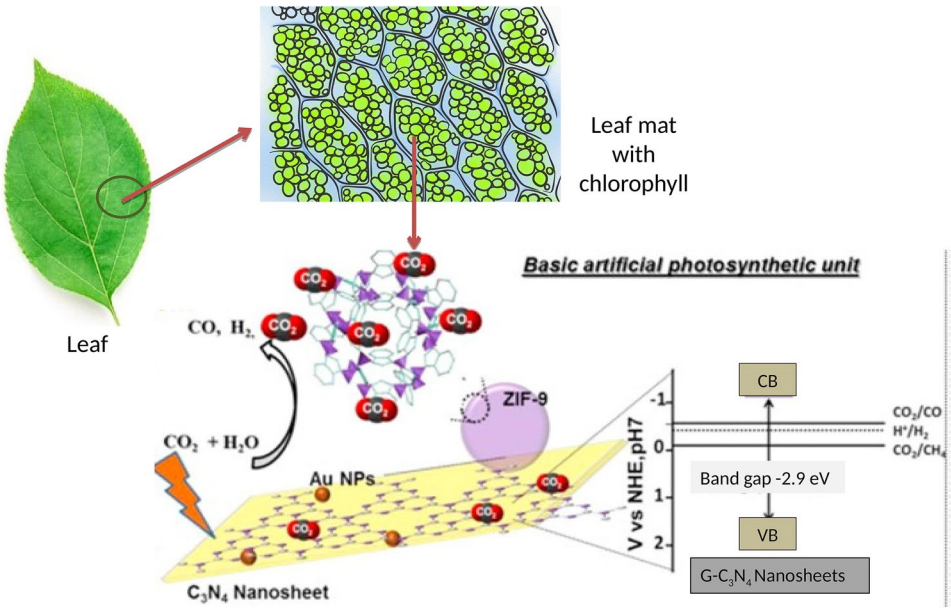

Fig. 12 Design and mechanistic of artificial photosynthetic utility [257]

nicotinamide adenine dinucleotide phosphate (NADP) to NADPH acts as an electron transporter and helps to convert the photon energy into chemical energy [264–266].

In another study, artificial moth eye structure was fabricated through the impregnation of perovskite on the glass frame which was coated with a layer of polydimethylsiloxane (PDMS) and phenyl-C61-butyric acid methyl ester (PCBM), while Ag was introduced as co-catalyst to enhance the trapping and scattering of low-energy photons. This moth eye framework provided a dramatic enhancement in the external quantum efficiency. Meanwhile, free absorption of electromagnetic spectrum was obtained which improved the surface plasmon resonance activity [267, 268]. Thus, above-discussed nature inspired nanostructure harbored with carbonaceous materials, surface modified semiconductors, and noble metal would be a new future perspective to devise intelligent energy materials.

Conclusion

The review has emphasized the distinct mechanistic features of nanostructure materials that lend them unique properties with potential benefits towards energy and environment. Though all nanostructure materials are potent for the purpose, the metal oxides established its excellent photostability after being modified through doping. The doping has expanded the absorption of the solar light that promoted water splitting and CO_2 reduction. It was clearly seen that the hydrothermal synthesis method can encompass the synthesis of various nanostructure materials such as zero-D, one-D, two-D, and three-D, and bring down the synthesis cost. Thus, the nanostructured materials have offered an economically feasible route for upgrading the technological approach. Meanwhile, biomimicking of nanostructure materials on the principle of nature's design also provided a pathway to solve the critical challenges of engineering and technology to develop highly intelligent and smart designs.

Acknowledgements The corresponding author is grateful to Science and Engineering Research Board, Department of Science and Technology (DST-SERB) for the financial support received under Early Career Research Award with grant code ECR/2016/001400.

Author's Contribution A. Rani, R. Reddy, U. Sharma, P. Mukerjee, P. Mishra, A. Kuila, and L.C. Sim have contributed equally.

Compliance with ethical standards

Conflict of interest The authors declare that they have no conflict of interest.

Open Access This article is distributed under the terms of the Creative Commons Attribution 4.0 International License (http://creativecommons.org/licenses/by/4.0/), which permits unrestricted use, distribution, and reproduction in any medium, provided you give appropriate credit to the original author(s) and the source, provide a link to the Creative Commons license, and indicate if changes were made.

References

1. Sagadevan, S.: Recent trends on nanostructures based solar energy applications: a review. Rev. Adv. Mater. Sci. **34**, 44–61 (2013)
2. Martha, S., Sahoo, P.C., Parida, K.M.: An overview on visible light responsive metal oxide based photocatalysts for hydrogen energy production. Rsc Adv. **5**, 61535–61553 (2015)

3. Li, H., Zhou, Y., Tu, W., Ye, J., Zou, Z.: State-of-the-art progress in diverse heterostructured photocatalysts toward promoting photocatalytic performance. Adv. Funct. Mater. **25**, 998–1013 (2015)
4. Li, H., Tu, W., Zhou, Y., Zou, Z.: Z-Scheme photocatalytic systems for promoting photocatalytic performance: recent progress and future challenges. Adv. Sci. **3**, Article ID:1500389, (2016)
5. Ohtani, B.: Photocatalysis A to Z—what we know and what we do not know in a scientific sense. J. Photochem. Photobiol. C: Photochem. Rev. **11**, 157–178 (2010)
6. Pallavi, N., Shivaraju, H.P.: A feasibility study on photocatalytic degradation of methyl benzene using N doped TiO_2 nanoparticles. Int. J. Nanotechnol. **14**, 762–774 (2017)
7. Satheesh, R., Vignesh, K., Suganthi, A., Rajarajan, M.: Visible light responsive photocatalytic applications of transition metal (M = Cu, Ni and Co) doped α-Fe_2O_3 nanoparticles. J. Environ. Chem. Eng. **2**, 1956–1968 (2014)
8. Ahmad, J., Majid, K.: In-situ synthesis of visible-light responsive Ag_2O/graphene oxide nanocomposites and effect of graphene oxide content on its photocatalytic activity. Adv. Compos. Hyb. Mater. **1**, 374–388 (2018)
9. Rajabi, H.R., Khani, O., Shamsipur, M., Vatanpour, V.: High-performance pure and Fe^{3+}-ion doped ZnS quantum dots as green nanophotocatalysts for the removal of malachite green under UV-light irradiation. J. Hazard. Mater. **250**, 370–378 (2013)
10. Sathishkumar, P., Sweena, R., Wu, J.J., Anandan, S.: Synthesis of CuO-ZnO nanophotocatalyst for visible light assisted degradation of a textile dye in aqueous solution. Chem. Eng. J. **171**, 136–140 (2011)
11. Sim, L.C., Wong, J.L., Hak, C.H., Tai, J.Y., Leong, K.H., Saravanan, P.: Sugarcane juice derived carbon dot–graphitic carbon nitride composites for bisphenol A degradation under sunlight irradiation. Beilstein J. Nanotechnol. **9**, 353–363 (2018)
12. Dionysiou, D.D., Khodadoust, A.P., Kern, A.M., Suidan, M.T., Baudin, I., Laîné, J.M.: Continuous-mode photocatalytic degradation of chlorinated phenols and pesticides in water using a bench-scale TiO_2 rotating disk reactor. Appl. Catal. B: Environ. **24**, 139–155 (2000)
13. Ayodhya, D., Veerabhadram, G.: A review on recent advances in photodegradation of dyes using doped and heterojunction based semiconductor metal sulfide nanostructures for environmental protection. Mater. Today Energy **9**, 83–113 (2018)
14. Chen, X., Shen, S., Guo, L., Mao, S.S.: Semiconductor-based photocatalytic hydrogen generation. Chem. Rev. **110**, 6503–6570 (2010)
15. Maida, K.: Z-scheme water splitting using two different semiconductor photocatalysts. ACS Catal. **3**, 1486–1503 (2013)
16. Valiev, R.: Materials science: nanomaterial advantage. Nature **419**, 887–889 (2002)
17. Guo, D., Xie, G., Luo, J.: Mechanical properties of nanoparticles: basics and applications. J. Phys. D. **47**, Article ID:013001, 25 (2014)
18. Gleiter, H.: Nanostructured materials: basic concepts and microstructure. Acta Mater. **48**, 1–29 (2000)
19. Gentile, A., Ruffino, F., Grimaldi, M. G.: Complex-morphology metal-based nanostructures: fabrication, characterization, and applications. Nanomaterials. **6**, Article ID:110, 33 (2016)
20. Burda, C., Lou, Y., Chen, X., Samia, A.C., Stout, J., Gole, J.L.: Enhanced nitrogen doping in TiO_2 nanoparticles. Nano Lett. **3**, 1049–1051 (2003)
21. Hensel, J., Wang, G., Li, Y., Zhang, J.Z.: Synergistic effect of CdSe quantum dot sensitization and nitrogen doping of TiO_2 nanostructures for photoelectrochemical solar hydrogen generation. Nano Lett. **10**, 478–483 (2010)
22. Yoshida, T., Niimi, S., Yamamoto, M., Nomoto, T., Yagi, S.: Effective nitrogen doping into TiO_2 (N-TiO_2) for visible light response photocatalysis. J. Colloid Interface Sci. **447**, 278–281 (2015)
23. Shi, R., Li, Z., Yu, H., Shang, L., Zhou, C., Waterhouse, G.I., Wu, L., Zhang, T.: Effect of nitrogen doping level on the performance of N-doped carbon quantum dot/TiO_2 composites for photocatalytic hydrogen evolution. Chem Sus Chem. **10**, 4650–4656 (2017)
24. Shin, S.W., Lee, J.Y., Ahn, K.S., Kang, S.H., Kim, J.H.: Visible light absorbing TiO_2 nanotube arrays by sulfur treatment for photoelectrochemical water splitting. J. Phys. Chem. C **119**, 13375–13383 (2015)
25. Lei, X.F., Xue, X.X., Yang, H., Chen, C., Li, X., Niu, M.C., Gao, X.Y., Yang, Y.T.: Effect of calcination temperature on the structure and visible-light photocatalytic activities of (N, S and C) co-doped TiO_2 nano-materials. Appl. Surf. Sci. **332**, 172–180 (2015)
26. Yan, X., Yuan, K., Lu, N., Xu, H., Zhang, S., Takeuchi, N., Kobayashi, H., Li, R.: The interplay of sulfur doping and surface hydroxyl in band gap engineering: mesoporous sulfur-doped TiO_2 coupled with magnetite as a recyclable, efficient, visible light active photocatalyst for water purification. Appl Catal B: Environ. **218**, 20–31 (2017)
27. Bakar, S.A., Ribeiro, C.: A comparative run for visible-light-driven photocatalytic activity of anionic and cationic S-doped TiO_2 photocatalysts: a case study of possible sulfur doping through chemical protocol. J. Mol. Catal. A: Chem. A: Chem. **421**, 1–15 (2016)
28. El-Sheikh, S.M., Zhang, G., El-Hosainy, H.M., Ismail, A.A., O'Shea, K.E., Falaras, P., Kontos, A.G., Dionysiou, D.D.: High performance sulfur, nitrogen and carbon doped mesoporous anatase–brookite TiO_2 photocatalyst for the removal of microcystin-LR under visible light irradiation. J. Hazard. Mater. **280**, 723–733 (2014)
29. Mollavali, M., Falamaki, C., Rohani, S.: Preparation of multiple-doped TiO_2 nanotube arrays with nitrogen, carbon and nickel with enhanced visible light photoelectrochemical activity via single-step anodization. Int. J. Hydrogen Energy **40**, 12239–12252 (2015)
30. Lu, Z., Zeng, L., Song, W., Qin, Z., Zeng, D., Xie, C.: In situ synthesis of C-TiO_2/g-C_3N_4 heterojunction nanocomposite as highly visible light active photocatalyst originated from effective interfacial charge transfer. Appl. Catal. B: Environ. **202**, 489–499 (2017)
31. Zhang, Y., Zhao, Z., Chen, J., Cheng, L., Chang, J., Sheng, W., Hu, C., Cao, S.: C-doped hollow TiO_2 spheres: in situ synthesis, controlled shell thickness, and superior visible-light photocatalytic activity. Appl. Catal. B: Environ. **165**, 715–722 (2015)
32. Ji, L., Zhang, Y., Miao, S., Gong, M., Liu, X.: In situ synthesis of carbon doped TiO_2 nanotubes with an enhanced photocatalytic performance under UV and visible light. Carbon **125**, 544–550 (2017)
33. Kerkez-Kuyumcu, Ö., Kibar, E., Dayıoğlu, K., Gedik, F., Akın, A.N., Özkara-Aydınoğlu, Ş.: A comparative study for removal of different dyes over M/TiO2 (M = Cu, Ni Co, Fe, Mn and Cr) photocatalysts under visible light irradiation. J. Photochem. Photobiol. A Chem. **311**, 176–185 (2015)
34. Inturi, S.N.R., Boningari, T., Suidan, M., Smirniotis, P.G.: Visible-light-induced photodegradation of gas phase acetonitrile using aerosol-made transition metal (V, Cr, Fe Co, Mn, Mo, Ni, Cu, Y, Ce, and Zr) doped TiO_2. Appl. Catal. B: Environ. **144**, 333–342 (2014)
35. Yan, X., Xue, C., Yang, B., Yang, G.: Novel three-dimensionally ordered macroporous Fe^{3+}-doped TiO_2 photocatalysts for H_2 production and degradation applications. Appl. Surf. Sci. **394**, 248–257 (2017)

36. Wang, G., Ma, X., Wei, S., Li, S., Qiao, J., Wang, J., Song, Y.: Highly efficient visible-light driven photocatalytic hydrogen production from a novel Z-scheme Er^{3+}: $yAlO_3/Ta_2O_5$-$V5^+$||Fe^{3+}-TiO_2/Au coated composite. J Power Sour. **373**, 161–171 (2018)
37. Xiang, G., Yu, Z., Hou, Y., Chen, Y., Peng, Z., Sun, L., Sun, L.: Simulated solar-light induced photoelectrocatalytic degradation of bisphenol-A using Fe^{3+}-doped TiO_2 nanotube arrays as a photoanode with simultaneous aeration. Sep. Purif. Technol. **161**, 144–151 (2016)
38. Arellano, U., Wang, J.A., Asomoza, M., Chen, L.F., González, J., Manzo, A., Solis, S., Lara, V.H.: Crystalline structure, surface chemistry and catalytic properties of Fe^{3+} doped TiO_2 sol–gel catalysts for photooxidation of 2, 4–dichlorophenoxyacetic acid. Mater. Chem. Phys. **214**, 247–259 (2018)
39. Devi, L.G., Murthy, B.N., Kumar, S.G.: Photocatalytic activity of V^{5+}, Mo^{6+} and Th^{4+} doped polycrystalline TiO_2 for the degradation of chlorpyrifos under UV/solar light. J. Mol. Catal. A: Chem. **308**, 174–181 (2009)
40. Ren, F., Li, H., Wang, Y., Yang, J.: Enhanced photocatalytic oxidation of propylene over V-doped TiO_2 photocatalyst: reaction mechanism between V^{5+} and single-electron-trapped oxygen vacancy. Appl. Catal. B Enviro. **176**, 160–172 (2015)
41. Chen, R.F., Zhang, C.X., Deng, J., Song, G.Q.: Preparation and photocatalytic activity of Cu^{2+}-doped TiO_2/SiO_2. Int. J. Miner. Metall. Mater. **16**, 220–225 (2009)
42. Zhang, M., Yuan, S., Wang, Z., Zhao, Y., Shi, L.: Photoelectrocatalytic properties of Cu^{2+}-doped TiO_2 film under visible light. Appl. Catal. B Environl. **134**, 185–192 (2013)
43. Wu, Z., Jin, R., Wang, H., Liu, Y.: Effect of ceria doping on SO_2 resistance of Mn/TiO_2 for selective catalytic reduction of NO with NH_3 at low temperature. Catal. Commun. **10**, 935–939 (2009)
44. Silva, A.M., Silva, C.G., Dražić, G., Faria, J.L.: Ce-doped TiO_2 for photocatalytic degradation of chlorophenol. Catal. Today **144**, 13–18 (2009)
45. Zhang, K., Guo, L.: Metal sulphide semiconductors for photocatalytic hydrogen production. Catal. Sci. Technol. **3**, 1672–1690 (2013)
46. Liang, Y.C., Wang, C.C.: Surface crystal feature-dependent photoactivity of ZnO–ZnS composite rods via hydrothermal sulfidation. RSC Adv. **8**, 5063–5070 (2018)
47. Shown, I., Samireddi, S., Chang, Y.C., Putikam, R., Chang, P.H., Sabbah, A., Fu, F.Y., Chen, W.F., Wu, C.I., Yu, T.Y., Chung, P.W., Lin, M.C., Chen, L.C., Chen, K.H.: Carbon-doped SnS_2 nanostructure as a high-efficiency solar fuel catalyst under visible light. Nat. Commun. **9**, 1–10 (2018)
48. Cho, K.M., Kim, K.H., Park, K., Kim, C., Kim, S., Al-Saggaf, A., Gereige, I., Jung, H.T.: Amine-functionalized graphene/CdS composite for photocatalytic reduction of CO_2. ACS Catal. **7**, 7064–7069 (2017)
49. Ohmori, T., Mametsuka, H., Suzuki, E.: Photocatalytic hydrogen evolution on InP suspension with inorganic sacrificial reducing agent. Int. J. Hydrogen Energy **25**, 953–955 (2000)
50. Li, Q., Zheng, M., You, Y., Liu, P., Ma, L., Shen, W.: Pt nanoparticle decorated InP nanopore arrays for enhanced photoelectrochemical performance. J. Alloys Compd. **736**, 80–86 (2018)
51. Cao, S., Chen, Y., Wang, C.J., He, P., Fu, W.F.: Highly efficient photocatalytic hydrogen evolution by nickel phosphide nanoparticles from aqueous solution. Chem. Commun. **50**, 10427–10429 (2014)
52. Holmes, M.A., Townsend, T.K., Osterloh, F.E.: Quantum confinement controlled photocatalytic water splitting by suspended CdSe nanocrystals. Chem. Commun. **48**, 371–373 (2012)
53. Yao, W.T., Yu, S.H., Liu, S.J., Chen, J.P., Liu, X.M., Li, F.Q.: Architectural control syntheses of CdS and CdSe nanoflowers, branched nanowires, and nanotrees via a solvothermal approach in a mixed solution and their photocatalytic property. J. Phys. Chem. B. **110**, 11704–11710 (2006)
54. Kaviyarasu, K., Ayeshamariam, A., Manikandan, E., Kennedy, J., Ladchumananandasivam, R., Gomes, U.U., Jayachandran, M., Maaza, M.: Solution processing of CuSe quantum dots: photocatalytic activity under RhB for UV and visible-light solar irradiation. Mater. Sci. Eng. B **210**, 1–9 (2016)
55. Shi, W., Shi, J., Yu, S., Liu, P.: Ion-exchange synthesis and enhanced visible-light photocatalytic activities of CuSe-ZnSe flower-like nanocomposites. Appl. Catal. B **138**, 184–190 (2013)
56. Cao, F., Shi, W., Zhao, L., Song, S., Yang, J., Lei, Y., Zhang, H.: Hydrothermal synthesis and high photocatalytic activity of 3D wurtzite ZnSe hierarchical nanostructures. J. Phys. Chem. C **112**, 17095–17101 (2008)
57. Chen, Y., Liang, S., Wen, L., Wu, W., Yuan, R., Wang, X., Wu, L.: A TaON nano-photocatalyst with low surface reduction defects for effective mineralization of chlorophenols under visible light irradiation. Phys. Chem. Chem. Phys. **15**, 12742–12747 (2013)
58. Hitoki, G., Takata, T., Kondo, J. N., Hara, M., Kobayashi, H., Domen, K.: An oxynitride, TaON, as an efficient water oxidation photocatalyst under visible light irradiation ($\lambda \leq 500$ nm). Chem. Commun. 1698–1699 (2002)
59. Hayashi, T., Deura, M., Ohkawa, K.: High stability and efficiency of GaN photocatalyst for hydrogen generation from water. Jpn. J. Appl. Phys. **51**, Article ID:112601, 3 (2012)
60. Ohkawa, K., Ohara, W., Uchida, D., Deura, M.: Highly stable GaN photocatalyst for producing H_2 gas from water. Jpn. J. Appl. Phys. **52**, Article ID: 08JH4, 3 (2013)
61. Maeda, K., Saito, N., Lu, D., Inoue, Y., Domen, K.: Photocatalytic properties of RuO_2-loaded β-Ge_3N_4 for overall water splitting. J. Phys. Chem. C **111**, 4749–4755 (2007)
62. Maeda, K., Domen, K.: New non-oxide photocatalysts designed for overall water splitting under visible light. J. Phys. Chem. C **111**, 7851–7861 (2007)
63. Lu, J., Wang, Y., Liu, F., Zhang, L., Chai, S.: Fabrication of a direct Z-scheme type WO_3/Ag_3PO_4 composite photocatalyst with enhanced visible-light photocatalytic performances. Appl. Surf. Sci. **393**, 180–190 (2017)
64. Dong, R., Tian, B., Zeng, C., Li, T., Wang, T., Zhang, J.: Ecofriendly synthesis and photocatalytic activity of uniform cubic Ag@AgCl plasmonic photocatalyst. J. Phys. Chem. C **117**, 213–220 (2012)
65. Kuai, L., Geng, B., Chen, X., Zhao, Y., Luo, Y.: Facile subsequently light-induced route to highly efficient and stable sunlight-driven Ag–AgBr plasmonic photocatalyst. Langmuir **26**, 18723–18727 (2010)
66. Kanhere, P., Chen, Z.: A review on visible light active perovskite-based photocatalysts. Molecules **19**, 19995–20022 (2014)
67. Shi, J., Guo, L.: ABO_3-based photocatalysts for water splitting. Progress Nat. Sci. Met. Mater. Int. Metals. **22**, 592–615 (2012)
68. Mutalib, M.A., Aziz, F., Jamaludin, N.A., Yahya, N., Ismail, A.F., Mohamed, M.A., Yusop, M.Z.M., Salleh, W.N.W., Jafar, J., Yusof, N.: Enhancement in photocatalytic degradation of methylene blue by LaFeO 3-GO integrated photocatalyst-adsorbents under visible light irradiation. Korean J. Chem. Eng. **35**, 548–556 (2018)
69. Han, X., Li, S., Peng, Z., Al-Yuobi, A.O., Bashammakh, A.S.O., El-Shahawi, M.S., Leblanc, R.M.: Interactions between carbon nanomaterials and biomolecules. J. Oleo Sci. **65**, 1–7 (2016)
70. Chai, B., Peng, T., Zhang, X., Mao, J., Li, K., Zhang, X.: Synthesis of C_{60}-decorated SWCNTs (C_{60}-d-CNTs) and its TiO_2-based nanocomposite with enhanced photocatalytic activity for hydrogen production. Dalton Trans. **42**, 3402–3409 (2013)

71. Anctil, A., Babbitt, C.W., Raffaelle, R.P., Landi, B.J.: Material and energy intensity of fullerene production. Environ. Sci. Technol. **45**, 2353–2359 (2011)
72. Fang, Y., Bi, C., Wang, D., Huang, J.: The functions of fullerenes in hybrid perovskite solar cells. ACS Energy Lett. **2**, 782–794 (2017)
73. Long, Y., Lu, Y., Huang, Y., Peng, Y., Lu, Y., Kang, S.Z., Mu, J.: Effect of C_{60} on the photocatalytic activity of TiO_2 nanorods. J. Phys. Chem. C **113**, 13899–13905 (2009)
74. Meng, Z.D., Peng, M.M., Zhu, L., Oh, W.C., Zhang, F.J.: Fullerene modification CdS/TiO_2 to enhancement surface area and modification of photocatalytic activity under visible light. Appl. Catal. B **113**, 141–149 (2012)
75. Yu, J., Ma, T., Liu, G., Cheng, B.: Enhanced photocatalytic activity of bimodal mesoporous titania powders by C_{60} modification. Dalton Trans. **40**, 6635–6644 (2011)
76. Yu, H., Shi, R., Zhao, Y., Waterhouse, G.I., Wu, L.Z., Tung, C.H., Zhang, T.: Smart utilization of carbon dots in semiconductor photocatalysis. Adv. Mater. **28**, 9454–9477 (2016)
77. Zhang, H., Huang, H., Ming, H., Li, H., Zhang, L., Liu, Y., Kang, Z.: Carbon quantum dots/Ag_3PO_4 complex photocatalysts with enhanced photocatalytic activity and stability under visible light. J. Mater. Chem. **22**, 10501–10506 (2012)
78. Wang, H., Yan, X., Piao, G.: A high-performance supercapacitor based on fullerene C_{60} whisker and polyaniline emeraldine base composite. Electrochim. Acta **231**, 264–271 (2017)
79. Kumar, V.B., Borenstein, A., Markovsky, B., Aurbach, D., Gedanken, A., Talianker, M., Porat, Z.: Activated carbon modified with carbon nanodots as novel electrode material for supercapacitors. J. Phys. Chem. C **120**, 13406–13413 (2016)
80. Zhu, T., Wu, H.B., Wang, Y., Xu, R., Lou, X.W.D.: Formation of 1D hierarchical structures composed of Ni_3S_2 nanosheets on CNTs backbone for supercapacitors and photocatalytic H_2 production. Adv. Energy Mater. **2**, 1497–1502 (2012)
81. Xia, X.H., Jia, Z.J., Yu, Y., Liang, Y., Wang, Z., Ma, L.L.: Preparation of multi-walled carbon nanotube supported TiO_2 and its photocatalytic activity in the reduction of CO_2 with H_2O. Carbon **45**, 717–721 (2007)
82. Li, Z., Gao, B., Chen, G.Z., Mokaya, R., Sotiropoulos, S., Puma, G.L.: Carbon nanotube/titanium dioxide (CNT/TiO_2) core–shell nanocomposites with tailored shell thickness, CNT content and photocatalytic/photoelectrocatalytic properties. Appl. Catal. B: Environmental. **110**, 50–57 (2011)
83. Mohamed, A., Yousef, S., Abdelnaby, M.A., Osman, T.A., Hamawandi, B., Toprak, M.S., Muhammed, M., Uheida, A.: Photocatalytic degradation of organic dyes and enhanced mechanical properties of PAN/CNTs composite nanofibers. Sep. Purif. Technol. **182**, 219–223 (2017)
84. Jia, J., Li, D., Wan, J., Yu, X.: Characterization and mechanism analysis of graphite/C-doped TiO_2 composite for enhanced photocatalytic performance. J. Ind. Eng. Chem. **33**, 162–169 (2016)
85. Chang, C.J., Chu, K.W., Hsu, M.H., Chen, C.Y.: Ni-doped ZnS decorated graphene composites with enhanced photocatalytic hydrogen-production performance. Int. J. Hydrogen Energy **40**, 14498–14506 (2015)
86. Zhang, Y., Tang, Z.R., Fu, X., Xu, Y.J.: TiO_2–graphene nanocomposites for gas-phase photocatalytic degradation of volatile aromatic pollutant: is TiO_2–graphene truly different from other TiO_2–carbon composite materials? ACS Nano **4**, 7303–7314 (2010)
87. Upadhyay, R.K., Soin, N., Roy, S.S.: Role of graphene/metal oxide composites as photocatalysts, adsorbents and disinfectants in water treatment: a review. Rsc Adv. **4**, 3823–3851 (2014)
88. Alam, U., Fleisch, M., Kretschmer, I., Bahnemann, D., Muneer, M.: One-step hydrothermal synthesis of Bi-TiO_2 nanotube/graphene composites: an efficient photocatalyst for spectacular degradation of organic pollutants under visible light irradiation. Appl. Catal. B: Environm. **218**, 758–769 (2017)
89. Ahmed, N., Farghali, A.A., El Rouby, W.M., Allam, N.K.: Enhanced photoelectrochemical water splitting characteristics of TiO_2 hollow porous spheres by embedding graphene as an electron transfer channel. Int. J. Hydrogen Energy **42**, 29131–29139 (2017)
90. Liang, Y.T., Vijayan, B.K., Gray, K.A., Hersam, M.C.: Minimizing graphene defects enhances titania nanocomposite-based photocatalytic reduction of CO_2 for improved solar fuel production. Nano. Lett. **11**, 2865–2870 (2011)
91. Ong, W.J., Tan, L.L., Chai, S.P., Yong, S.T., Mohamed, A.R.: Self-assembly of nitrogen-doped TiO2 with exposed 001 facets on a graphene scaffold as photo-active hybrid nanostructures for reduction of carbon dioxide to methane. Nano Res. **7**, 1528–1547 (2014)
92. Trapalis, A., Todorova, N., Giannakopoulou, T., Boukos, N., Speliotis, T., Dimotikali, D., Yu, J.: TiO_2/graphene composite photocatalysts for NO_x removal: a comparison of surfactant-stabilized graphene and reduced graphene oxide. Appl. Catal. B Environ. **180**, 637–647 (2016)
93. Som, T., Troppenz, G.V., Wendt, R., Wollgarten, M., Rappich, J., Emmerling, F., Rademann, K.: Graphene oxide/α-Bi_2O_3 composites for visible-light photocatalysis, chemical catalysis, and solar energy conversion. Chemsuschem **7**, 854–865 (2014)
94. Yeh, T.F., Teng, C.Y., Chen, S.J., Teng, H.: Nitrogen-doped graphene oxide quantum dots as photocatalysts for overall water-splitting under visible light illumination. Adv. Mater. **26**, 3297–3303 (2014)
95. Yu, J., Jin, J., Cheng, B., Jaroniec, M.: A noble metal-free reduced graphene oxide–CdS nanorod composite for the enhanced visible-light photocatalytic reduction of CO_2 to solar fuel. J. Mater. Chem. A. **2**, 3407–3416 (2014)
96. Iwashina, K., Iwase, A., Ng, Y.H., Amal, R., Kudo, A.: Z-schematic water splitting into H_2 and O_2 using metal sulfide as a hydrogen-evolving photocatalyst and reduced graphene oxide as a solid-state electron mediator. J. Am. Chem. Soc. **137**, 604–607 (2015)
97. Zhang, Y., Zhu, Y., Yu, J., Yang, D., Ng, T.W., Wong, P.K., Jimmy, C.Y.: Enhanced photocatalytic water disinfection properties of Bi_2MoO_6–RGO nanocomposites under visible light irradiation. Nanoscale. **5**, 6307–6310 (2013)
98. Reddy, K.R., Hassan, M., Gomes, V.G.: Hybrid nanostructures based on titanium dioxide for enhanced photocatalysis. Appl. Catal. A Gen. **489**, 1–16 (2015)
99. Zhu, Y.P., Ren, T.Z., Yuan, Z.Y.: Mesoporous phosphorus-doped g-C_3N_4 nanostructured flowers with superior photocatalytic hydrogen evolution performance. ACS Appl. Mater. Interfaces. **7**, 16850–16856 (2015)
100. Xiong, T., Cen, W., Zhang, Y., Dong, F.: Bridging the g-C_3N_4 interlayers for enhanced photocatalysis. Acs. Catal. **6**, 2462–2472 (2016)
101. Mohamed, M.A., Zain, M.F.M., Minggu, L.J., Kassim, M.B., Amin, N.A.S., Salleh, W.N.W., Salehmin, M.N.I., Nasir, M.F.M., Hir, Z.A.M.: Constructing bio-templated 3D porous microtubular C-doped g-C_3N_4 with tunable band structure and enhanced charge carrier separation. Applied Appl. Catal. B Environ. **236**, 265–279 (2018)
102. Chang, C., Fu, Y., Hu, M., Wang, C., Shan, G., Zhu, L.: Photodegradation of bisphenol A by highly stable palladium-doped mesoporous graphite carbon nitride (Pd/mpg-C_3N_4) under simulated solar light irradiation. Appl. Catal. B Environm. **142**, 553–560 (2013)
103. Zong, X., Miao, X., Hua, S., An, L., Gao, X., Jiang, W., Qu, D., Zhou, Z., Liu, X., Sun, Z.: Structure defects assisted

photocatalytic H_2 production for polythiophene nanofibers. Appl. Catal. B: Environ. **211**, 98–105 (2017)
104. Shahabuddin, S., Khanam, R., Khalid, M., Sarih, N.M., Ching, J.J., Mohamad, S., Saidur, R.: Synthesis of 2D boron nitride doped polyaniline hybrid nanocomposites for photocatalytic degradation of carcinogenic dyes from aqueous solution. Arab. J. Chem. (2018) **(in press)**
105. Nor, N.A.M., Jaafar, J., Ismail, A.F., Mohamed, M.A., Rahman, M.A., Othman, M.H.D., Lau, W.J., Yusof, N.: Preparation and performance of PVDF-based nanocomposite membrane consisting of TiO_2 nanofibers for organic pollutant decomposition in wastewater under UV irradiation. Desalination **391**, 89–97 (2016)
106. Hir, Z.A.M., Moradihamedani, P., Abdullah, A.H., Mohamed, M.A.: Immobilization of TiO_2 into polyethersulfone matrix as hybrid film photocatalyst for effective degradation of methyl orange dye. Mater. Sci. Semicond. Process. **57**, 157–165 (2017)
107. Hir, Z.A.M., Abdullah, A.H., Zainal, Z., Lim, H.N.: Visible light-active hybrid film photocatalyst of polyethersulfone–reduced TiO_2: photocatalytic response and radical trapping investigation. J. Mater. Sci. **53**, 13264–13279 (2018)
108. Mohd Hir, Z.A., Abdullah, A.H., Zainal, Z., Lim, H.N.: Photoactive hybrid film photocatalyst of polyethersulfone-ZnO for the degradation of methyl orange dye: kinetic study and operational parameters. Catalysts. **7**, 313 (2017)
109. Mohamed, M.A., Salleh, W.N.W., Jaafar, J., Ismail, A.F., Mutalib, M.A., Sani, N.A.A., Asri, S.E.A.M., Ong, C.S.: Physicochemical characteristic of regenerated cellulose/N-doped TiO_2 nanocomposite membrane fabricated from recycled newspaper with photocatalytic activity under UV and visible light irradiation. Open Chem. Eng. J. Open. **284**, 202–215 (2016)
110. Mohamed, M.A., Mutalib, M.A., Hir, Z.A.M., Zain, M.F.M., Mohamad, A.B., Minggu, L.J., Awang, N.A., Salleh, W.N.W.: An overview on cellulose-based material in tailoring bio-hybrid nanostructured photocatalysts for water treatment and renewable energy applications. Int. J. Biol. Macromol. **103**, 1232–1256 (2017)
111. Maeda, K., Domen, K.: Photocatalytic water splitting: recent progress and future challenges. J. Phys. Chem. Lett. **1**, 2655–2661 (2010)
112. Maeda, K., Teramura, K., Lu, D., Saito, N., Inoue, Y., Domen, K.: Noble-metal/Cr2O3 core/shell nanoparticles as a cocatalyst for photocatalytic overall water splitting. Angew. Chem. Int. Ed. **118**, 7970–7973 (2006)
113. Maeda, K., Sakamoto, N., Ikeda, T., Ohtsuka, H., Xiong, A., Lu, D., Kanehara, M., Teranjshi, T., Domen, K.: Preparation of core–shell-structured nanoparticles (with a noble-metal or metal oxide core and a chromia shell) and their application in water splitting by means of visible light. Chem. Eur. J. **16**, 7750–7759 (2010)
114. Wang, Y., Wang, Q., Zhan, X., Wang, F., Safdar, M., He, J.: Visible light driven type II heterostructures and their enhanced photocatalysis properties: a review. Nanoscale. **5**, 8326–8339 (2013)
115. Huang, L., Wang, X., Yang, J., Liu, G., Han, J., Li, C.: Dual cocatalysts loaded type I CdS/ZnS core/shell nanocrystals as effective and stable photocatalysts for H_2 evolution. J. Phys. Chem. C **117**, 11584–11591 (2013)
116. Li, T.B., Chen, G., Zhou, C., Shen, Z.Y., Jin, R.C., Sun, J.X.: New photocatalyst BiOCl/BiOI composites with highly enhanced visible light photocatalytic performances. Dalton Trans. **40**, 6751–6758 (2011)
117. Zhang, X., Zhang, L., Xie, T., Wang, D.: Low-temperature synthesis and high visible-light-induced photocatalytic activity of BiOI/TiO_2 heterostructures. J. Phys. Chem. C **113**, 7371–7378 (2009)
118. Di, T., Zhu, B., Cheng, B., Yu, J., Xu, J.: A direct Z-scheme g-C_3N_4/SnS_2 photocatalyst with superior visible-light CO_2 reduction performance. J. Catal. **352**, 532–541 (2017)
119. Shi, H., Chen, G., Zhang, C., Zou, Z.: Polymeric g-C_3N_4 coupled with $NaNbO_3$ nanowires toward enhanced photocatalytic reduction of CO_2 into renewable fuel. ACS Catal. **4**, 3637–3643 (2014)
120. Chen, Z., Wang, W., Zhang, Z., Fang, X.: High-efficiency visible-light-driven Ag_3PO_4/AgI photocatalysts: z-scheme photocatalytic mechanism for their enhanced photocatalytic activity. J. Phys. Chem. C. **117**, 19346–19352 (2013)
121. Zhang, L.J., Li, S., Liu, B.K., Wang, D.J., Xie, T.F.: Highly efficient CdS/WO_3 photocatalysts: z-scheme photocatalytic mechanism for their enhanced photocatalytic H_2 evolution under visible light. ACS Catal. **4**, 3724–3729 (2014)
122. Liu, X., Jin, A., Jia, Y., Xia, T., Deng, C., Zhu, M., Chen, C., Chen, X.: Synergy of adsorption and visible-light photocatalytic degradation of methylene blue by a bifunctional Z-scheme heterojunction of WO_3/g-C_3N_4. Appl. Surf. Sci. **405**, 359–371 (2017)
123. Jariwala, D.: Tunable confinement of charges and excitations. Nat. Nanotechnol. **13**, 99–100 (2018)
124. Chen, Q., Tong, R., Chen, X., Xue, Y., Xie, Z., Kuang, Q., Zheng, L.: Ultrafine ZnO quantum dot-modified TiO_2 composite photocatalysts: the role of the quantum size effect in heterojunction-enhanced photocatalytic hydrogen evolution. Catal. Sci. Technol. **8**, 1296–1303 (2018)
125. Islam, S.Z., Nagpure, S., Kim, D.Y., Rankin, S.E.: Synthesis and catalytic applications of non-metal doped mesoporous titania. Inorganics. **5**, 1–43 (2017)
126. Zhuang, H., Zhang, Y., Chu, Z., Long, J., An, X., Zhang, H., Lin, H., Zhang, Z., Wang, X.: Synergy of metal and nonmetal dopants for visible-light photocatalysis: a case-study of Sn and N co-doped TiO_2. Phys. Chem. Chem. Phys. **18**, 9636–9644 (2016)
127. Singh, Ch., Shaffer, M., Kinloch, I., Windle, A.: Production of aligned carbon nanotubes by the CVD injection method. Phys. B **323**, 339–340 (2002)
128. Sobczyk-Guzenda, A., Gazicki-Lipman, M., Szymanowski, H., Kowalski, J., Wojciechowski, P., Halamus, T., Tracz, A.: Characterization of thin TiO_2 films prepared by plasma enhanced chemical vapour deposition for optical and photocatalytic applications. Thin Solid Films **517**, 5409–5414 (2009)
129. Murgolo, S., Yargeau, V., Gerbasi, R., Visentin, F., El Habra, N., Ricco Lacchetti, I., Carere, M., Curri, M.L., Mascolo, G.: A new supported TiO_2 film deposited on stainless steel for the photocatalytic degradation of contaminants of emerging concern. Chem. Eng. J. **318**, 103–111 (2017)
130. Su, G., Hadjiev, V.G., Loya, P.E., Zhang, J., Lei, S., Maharjan, S., Dong, P., Ajayan, P.M., Lou, J., Peng, H.: Chemical vapor deposition of thin crystals of layered semiconductor SnS_2 for fast photodetection application. Nano Lett. **15**, 506–513 (2014)
131. Pawbake, A.S., Waykar, R.G., Late, D.J., Jadkar, S.R.: Highly transparent wafer-scale synthesis of crystalline WS_2 nanoparticle thin film for photodetector and humidity-sensing applications. ACS Appl. Mater. Interfaces. **8**, 3359–3365 (2016)
132. Shi, J., Tong, R., Zhou, X., Gong, Y., Zhang, Z., Ji, Q., Zhang, Y., Fang, Q., Gu, L., Wang, X., Liu, Z., Zhang, Y.: Temperature-mediated selective growth of MoS2/WS2 and WS2/MoS2 vertical stacks on au foils for direct photocatalytic applications. Adv. Mater. **28**, 10664–10672 (2016)
133. Chadwick, N., Sathasivam, S., Kafizas, A., Bawaked, S.M., Obaid, A.Y., Al-Thabaiti, S., Basahel, S.N., Parkin, I.P., Carmalt, C.J.: Combinatorial aerosol assisted chemical vapour deposition of a photocatalytic mixed SnO_2/TiO_2 thin film. J. Mater. Chem. A. **2**, 5108–5116 (2014)

134. Alotaibi, A.M., Sathasivam, S., Parkin, I.P.: Aerosol assisted chemical vapour deposition of a ZrO_2–TiO_2 composite thin film with enhanced photocatalytic activity. RSC Adv. **5**, 67944–67950 (2015)
135. Chavarría-Castillo, K.A., Amézaga-Madrid, P., Esquivel-Pereyra, O., Antúnez-Flores, W., Pizá Ruiz, P., Miki-Yoshida, M.: Synthesis and microstructural characterization of SnO_2: F thin films deposited by AACVD. Mater. Res. **19**, 97–102 (2016)
136. Lee, M.H., Park, Y.H., Yang, C.K.: Effects of pH and Temperature on sol–gel processing within the PbO–TiO_2 system. J. Am. Ceram. Soc. **70**, C-35 (1987)
137. Krishnan, J., Mohamad, E.N., Sikirman, A.: Effect of calcination temperature of carbon doped TiO_2 (C-TiO_2) on photocatalytic activity under visible light. Adv. Mater. Res. **997**, 292–296 (2014)
138. Lu, L., Li, L., Hu, T., Zhang, W., Huang, X., Zhang, J., Liu, X.: Preparation, characterization, and photocatalytic activity of three-dimensionally ordered macroporous hybrid monosubstituted polyoxometalate $K_5[Co(H_2O)\ PW_{11}O_{39}]$ amine functionalized titanium catalysts. J Mol Catal A Chem. Chem. **394**, 283–294 (2014)
139. Hayat, K., Gondal, M.A., Khaled, M.M., Ahmed, S., Shemsi, A.M.: Nano ZnO synthesis by modified sol gel method and its application in heterogeneous photocatalytic removal of phenol from water. Appl. Catal. A Gen. **393**, 122–129 (2011)
140. Palanisamy, B., Babu, C.M., Sundaravel, B., Anandan, S., Murugesan, V.: Sol–gel synthesis of mesoporous mixed Fe_2O_3/TiO_2 photocatalyst: application for degradation of 4-chlorophenol. J. Hazard. Mater. **252**, 233–242 (2013)
141. Ji, X., Wang, J., Mei, L., Tao, W., Barrett, A., Su, Z., Wang, S., Ma, G., Shi, J., Zhang, S.: Porphyrin/SiO_2/Cp* Rh (bpy) Cl Hybrid nanoparticles mimicking chloroplast with enhanced electronic energy transfer for biocatalyzed artificial photosynthesis. Adv. Funct. Mater. Article ID:1705083, 14 (2018)
142. Crişan, M., Drăgan, N., Crişan, D., Ianculescu, A., Niţoi, I., Oancea, P., Todan, L., Stan, C., Stănică, N.: The effects of Fe, Co and Ni dopants on TiO_2 structure of sol–gel nanopowders used as photocatalysts for environmental protection: a comparative study. Ceram. Int. **42**, 3088–3095 (2016)
143. Zhang, G., Lü, F., Li, M., Yang, J., Zhang, X., Huang, B.: Synthesis of nanometer Bi_2WO_6 synthesized by sol–gel method and its visible-light photocatalytic activity for degradation of 4BS. J. Phys. Chem. Solids **71**, 579–582 (2010)
144. Teoh, W.Y.: A perspective on the flame spray synthesis of photocatalyst nanoparticles. Materials **6**, 3194–3212 (2013)
145. Nemade, K.R., Waghuley, S.A.: Band gap engineering of CuS nanoparticles for artificial photosynthesis. Mater. Sci. Semicond. Process. **39**, 781–785 (2015)
146. Boningari, T., Inturi, S.N.R., Suidan, M., Smirniotis, P.G.: Novel one-step synthesis of sulfur doped-TiO_2 by flame spray pyrolysis for visible light photocatalytic degradation of acetaldehyde. Chem. Eng. J. **339**, 249–258 (2018)
147. Boningari, T., Inturi, S.N.R., Suidan, M., Smirniotis, P.G.: Novel continuous single-step synthesis of nitrogen-modified TiO_2 by flame spray pyrolysis for photocatalytic degradation of phenol in visible light. J. Mater. Sci. Technol. **34**, 1494–1502 (2018)
148. Xiong, Z., Lei, Z., Xu, Z., Chen, X., Gong, B., Zhao, Y., Zhao, H., Zhang, J., Zheng, C.: Flame spray pyrolysis synthesized ZnO/CeO_2 nanocomposites for enhanced CO_2 photocatalytic reduction under UV–Vis light irradiation. J. CO_2 Util. **18**, 53–61 (2017)
149. Borsella, E., D'Amato, R., Terranova, G., Falconieri, M., Fabbri, F.: Synthesis of nanoparticles by laser pyrolysis: from research to applications. ENEA Mag. **4**, 54–64 (2011)
150. Bouhadoun, S., Guillard, C., Herlin-Boime, N.: Gold and nitrogen co-doped TiO_2 nanoparticles synthesized by laser pyrolysis, application in photocatalysis. In: The 19th International conference on Semiconductor Photocatalysis and Solar Energy Conversion (SPASEC-19). (2014)
151. Bouhadoun, S., Guillard, C., Dapozze, F., Singh, S., Amans, D., Bouclé, J., Herlin-Boime, N.: One step synthesis of N-doped and Au-loaded TiO_2 nanoparticles by laser pyrolysis: application in photocatalysis. Appl. Catal. B Environ. **174**, 367–375 (2015)
152. Scarisoreanu, M., Fleaca, C., Morjan, I., Niculescu, A.M., Luculescu, C., Dutu, E., llie, A., Morjan, I., Florescu, L.G., Vasile, E., Fort, C.I.: High photoactive TiO_2/SnO_2 nanocomposites prepared by laser pyrolysis. Appl. Surf. Sci. **418**, 491–498 (2017)
153. Amin, G., Asif, M.H., Zainelabdin, A., Zaman, S., Nur, O., Willander, M.: Influence of pH, precursor concentration, growth time, and temperature on the morphology of ZnO nanostructures grown by the hydrothermal method. J. Nanomater. **2011**, Article ID 269692, 9 (2011)
154. Tian, Y., Chang, B., Lu, J., Fu, J., Xi, F., Dong, X.: Hydrothermal synthesis of graphitic carbon nitride–Bi_2WO_6 heterojunctions with enhanced visible light photocatalytic activities. ACS Appl. Mater. Interfaces. **5**, 7079–7085 (2013)
155. Huang, X., Chen, H.: One-pot hydrothermal synthesis of $Bi_2O_2CO_3$/Bi_2WO_6 visible light photocatalyst with enhanced photocatalytic activity. Appl. Surf. Sci. **284**, 843–848 (2013)
156. Liu, B., Lin, L., Yu, D., Sun, J., Zhu, Z., Gao, P., Wang, W.: Construction of fiber-based $BiVO_4$/SiO_2/reduced graphene oxide (RGO) with efficient visible light photocatalytic activity. Cellulose **25**, 1089–1101 (2018)
157. Ma, H., Shen, J., Shi, M., Lu, X., Li, Z., Long, Y., Li, N., Ye, M.: Significant enhanced performance for Rhodamine B, phenol and Cr(VI) removal by Bi_2WO_6 nanocomposites via reduced graphene oxide modification. Appl. Catal. B: Environ. **121**, 198–205 (2012)
158. Fakhri, A., Behrouz, S., Pourmand, M.: Synthesis, photocatalytic and antimicrobial properties of SnO_2, SnS_2 and SnO_2/SnS_2 nanostructure. J. Photochem. Photobiol. B Biol. **149**, 45–50 (2015)
159. Liu, S., Sun, H., Suvorova, A., Wang, S.: One-pot hydrothermal synthesis of ZnO-reduced graphene oxide composites using Zn powders for enhanced photocatalysis. Chem. Eng. J. **229**, 533–539 (2013)
160. Chaianansutcharit, S., Mekasuwandumrong, O., Praserthdam, P.: Effect of organic solvents on iron oxide nanoparticles by the solvothermal method. Cryst. Growth Des. **6**, 40–45 (2006)
161. Adschiri, T., Kanazawa, K., Arai, K.: Rapid and continuous hydrothermal crystallization of metal oxide particles in supercritical water. J. Am. Ceram. Soc. **75**, 1019–1022 (1992)
162. Zhou, Y., Luo, Q., Liu, Y., Li, D., Yang, L., Cao, F., Zhao, D.: Solvothermal synthesis of hollow flower-like Gd-doped TiO_2 with enhanced photocatalytic performance. J. Mater. Sci. Mater. Electron. **29**, 446–454 (2018)
163. Fan, Z., Meng, F., Zhang, M., Wu, Z., Sun, Z., Li, A.: Solvothermal synthesis of hierarchical TiO_2 nanostructures with tunable morphology and enhanced photocatalytic activity. Appl. Surf. Sci. **360**, 298–305 (2016)
164. Nguyen, T.D.: Solvothermal Synthesis of Bi_2WO_6 and its Photocatalytic Activity under Visible Light Irradiation. VJSTE. **54**, 42–47 (2016)
165. Moussa, H., Girot, E., Mozet, K., Alem, H., Medjahdi, G., Schneider, R.: ZnO rods/reduced graphene oxide composites prepared via a solvothermal reaction for efficient sunlight-driven photocatalysis. Appl. Catal. B: Environ. **185**, 11–21 (2016)
166. Wang, H.X., Wu, R., Wei, S.H., Yu, L.R., Jian, J.K., Hou, J., Wang, J., Zhang, H.Y., Sun, Y.F.: One-pot solvothermal synthesis of ZnTe/RGO nanocomposites and enhanced visible-light photocatalysis. Chin. Chem. Lett. **27**, 1572–1576 (2016)
167. Sun, T.W., Zhu, Y.J., Qi, C., Ding, G.J., Chen, F., Wu, J.: α-Fe_2O_3 nanosheet-assembled hierarchical hollow mesoporous microspheres: microwave-assisted solvothermal synthesis and

application in photocatalysis. J. Colloid Interface Sci. **463**, 107–117 (2016)
168. He, R., Cao, S., Yu, J., Yang, Y.: Microwave-assisted solvothermal synthesis of $Bi_4O_5I_2$ hierarchical architectures with high photocatalytic performance. Catal. Today **264**, 221–228 (2016)
169. Sun, T., Jiang, H.Y., Ma, C.C., Mao, F., Xue, B.: Ag/g-C_3N_4 photocatalysts: microwave-assisted synthesis and enhanced visible-light photocatalytic activity. Catal. Commun. **79**, 45–48 (2016)
170. Darwish, M., Mohammadi, A., Assi, N.: Microwave-assisted polyol synthesis and characterization of pvp-capped CdS nanoparticles for the photocatalytic degradation of tartrazine. Mater. Res. Bull. **74**, 387–396 (2016)
171. Nithya, V.D., Hanitha, B., Surendran, S., Kalpana, D., Selvan, R.K.: Effect of pH on the sonochemical synthesis of $BiPO_4$ nanostructures and its electrochemical properties for pseudocapacitors. Ultrason. Sonochem. **22**, 300–310 (2015)
172. Teh, C.Y., Wu, T.Y., Juan, J.C.: Facile sonochemical synthesis of N, Cl-codoped TiO_2: synthesis effects, mechanism and photocatalytic performance. Catal. Today **256**, 365–374 (2015)
173. Shende, T.P., Bhanvase, B.A., Rathod, A.P., Pinjari, D.V., Sonawane, S.H.: Sonochemical synthesis of Graphene-Ce-TiO_2 and Graphene-Fe-TiO_2 ternary hybrid photocatalyst nanocomposite and its application in degradation of Crystal Violet Dye. Ultrason. Sonochem. **41**, 582–589 (2018)
174. Dutta, D.P., Tyagi, A.K.: Facile sonochemical synthesis of Ag modified $Bi_4Ti_3O_{12}$ nanoparticles with enhanced photocatalytic activity under visible light. Mater. Res. Bull. **74**, 397–407 (2016)
175. Golsheikh, A.M., Lim, H.N., Zakaria, R., Huang, N.M.: Sonochemical synthesis of reduced graphene oxide uniformly decorated with hierarchical ZnS nanospheres and its enhanced photocatalytic activities. RSC Adv. **5**, 12726–12735 (2015)
176. Gholamrezaei, S., Salavati-Niasari, M.: Sonochemical synthesis of $SrMnO_3$ nanoparticles as an efficient and new catalyst for O_2 evolution from water splitting reaction. Ultrason. Sono. **40**, 651–663 (2018)
177. Dhand, C., Dwivedi, N., Loh, X.J., Ying, A.N.J., Verma, N.K., Beuerman, R.W., Lakshminarayanan, R., Ramakrishna, S.: Methods and strategies for the synthesis of diverse nanoparticles and their applications: a comprehensive overview. RSC Adv. **5**, 105003–105037 (2015)
178. Drmota, A., Drofenik, M., Koselj, J., Žnidaršič, A.: Microemulsion method for synthesis of magnetic oxide nanoparticles. In: Dr. Najjar, R. (Ed.) Microemulsions—An Introduction to Properties and Applications, pp. 191–214. InTech (2012)
179. Sanchez-Dominguez, M., Morales-Mendoza, G., Rodriguez-Vargas, M.J., Ibarra-Malo, C.C., Rodriguez-Rodriguez, A.A., Vela-Gonzalez, A.V., Perez-Garcia, S.A., Gomez, R.: Synthesis of Zn-doped TiO_2 nanoparticles by the novel oil-in-water (O/W) microemulsion method and their use for the photocatalytic degradation of phenol. J. Environ. Chem. Eng. **3**, 3037–3047 (2015)
180. Mao, D., Yu, A., Ding, S., Wang, F., Yang, S., Sun, C., He, H., Liu, Y., Yu, K.: One-pot synthesis of BiOCl half-shells using microemulsion droplets as templates with highly photocatalytic performance for the degradation of ciprofloxacin. Appl. Surf. Sci. **389**, 742–750 (2016)
181. Mao, D., Ding, S., Meng, L., Dai, Y., Sun, C., Yang, S., He, H.: One-pot microemulsion-mediated synthesis of Bi-rich Bi4O5Br 2 with controllable morphologies and excellent visible-light photocatalytic removal of pollutants. Appl. Catal. B: Environ. **207**, 153–165 (2017)
182. Emsaki, M., Hassanzadeh-Tabrizi, S.A., Saffar-Teluri, A.: Microemulsion synthesis of ZnO–$ZnWO_4$ nanoparticles for superior photodegradation of organic dyes in water. J. Mater. Sci. Mater. Electron. **29**, 2384–2391 (2018)
183. Wang, Y.H., Chiu, SCh., Lin, K.M., Li, Y.Y.: Formation of carbon nanotubes from polyvinyl alcohol using arc-discharge method. Carbon **42**, 2535–2541 (2004)
184. Ashkarran, A.A., Mohammadi, B.: ZnO nanoparticles decorated on graphene sheets through liquid arc discharge approach with enhanced photocatalytic performance under visible-light. Appl. Surf. Sci. **342**, 112–119 (2015)
185. Arikawati, E., Saraswati, T. E.: Preparation of amine-functionalized TiO_2/carbon photocatalyst by arc discharge in liquid. In: IOP Conference Series: J. Mater. Sci. Eng. IOP Publishing. **176**, Article ID:012045, 6 (2017)
186. MamathaKumari, M., Kumar, D.P., Haridoss, P., DurgaKumari, V., Shankar, M.V.: Nanohybrid of titania/carbon nanotubes–nanohorns: a promising photocatalyst for enhanced hydrogen production under solar irradiation. Int. J. Hydrogen Energy **40**, 1665–1674 (2015)
187. Avcı, A., Eskizeybek, V., Gülce, H., Haspulat, B., Şahin, Ö.S.: ZnO–TiO_2 nanocomposites formed under submerged DC arc discharge: preparation, characterization and photocatalytic properties. Appl. Phys. A **116**, 1119–1125 (2014)
188. Lee, Y.G., Wang, J.R., Chuang, M.J., Chen, D.W., Hou, K.H.: The effect of electrolyte temperature on the electrodeposition of cuprous oxide films. Int. J. Electrochem. Sci. **12**, 507–516 (2017)
189. Zhu, Z., Ren, Y., Li, Q., Liu, H., Weng, H.: One-pot electrodeposition synthesis of Bi_2WO_6/graphene composites for photocatalytic applications under visible light irradiation. Ceram. Int. **44**, 3511–3516 (2018)
190. Xu, X., Zhou, X., Li, X., Yang, F., Jin, B., Xu, T., Li, G., Li, M.: Electrodeposition synthesis of MnO_2/TiO_2 nanotube arrays nanocomposites and their visible light photocatalytic activity. Mater. Res. Bull. **59**, 32–36 (2014)
191. Karthikeyan, N., Sivaranjani, T., Dhanavel, S., Gupta, V.K., Narayanan, V., Stephen, A.: Visible light degradation of textile effluent by electrodeposited multiphase $CuInSe_2$ semiconductor photocatalysts. J. Mol. Liq. **227**, 194–201 (2017)
192. Zhu, T., Chong, M.N., Phuan, Y.W., Ocon, J.D., Chan, E.S.: Effects of electrodeposition synthesis parameters on the photoactivity of nanostructured tungsten trioxide thin films: optimisation study using response surface methodology. J. Taiwan Inst. Chem. Eng. **61**, 196–204 (2016)
193. He, J., Feng, H., Wang, T., Wang, T., Zeng, H.: Morphology-controlled electrodeposition of copper nanospheres onto FTO for enhanced photocatalytic hydrogen production. Chin. J. Chem. **36**, 31–36 (2018)
194. Chee, S.S., Lee, J. H.: Effects of pH on tin nanoparticles prepared using a modified polyol synthesis. In: Yahaya, M. (e. d.) Appl. Mech. Matt., pp. 93–96. Trans Tech Publications (2013)
195. Ma, L.L., Li, J.L., Sun, H.Z., Qiu, M.Q., Wang, J.B., Chen, J.Y., Yu, Y.: Self-assembled Cu_2O flowerlike architecture: polyol synthesis, photocatalytic activity and stability under simulated solar light. Mater. Res. Bull. **45**, 961–968 (2010)
196. Ikeda, T., Xiong, A., Yoshinaga, T., Maeda, K., Domen, K., Teranishi, T.: Polyol synthesis of size-controlled Rh nanoparticles and their application to photocatalytic overall water splitting under visible light. J. Phys. Chem. C **117**, 2467–2473 (2012)
197. Sasikala, R., Shirole, A., Sudarsan, V., Sakuntala, T., Sudakar, C., Naik, R., Bharadwaj, S.R.: Highly dispersed phase of SnO_2 on TiO_2 nanoparticles synthesized by polyol-mediated route: photocatalytic activity for hydrogen generation. Int. J. Hydrogen Energy **34**, 3621–3630 (2009)
198. Fu, W., Liu, M., Xue, F., Wang, X., Diao, Z., Guo, L.: Facile polyol synthesis of CuS nanocrystals with a hierarchical nanoplate structure and their application for electrocatalysis and photocatalysis. RSC Adv. **6**, 80361–80367 (2016)
199. Sun, Y., Cheng, H., Gao, S., Sun, Z., Liu, Q., Liu, Q., Lei, F., Yao, T., He, J., Wei, S., Xie, Y.: Freestanding tin disulfide

single-layers realizing efficient visible-light water splitting. Angew. Chem. Int. Ed. Angewandte. **51**, 8727–8731 (2012)
200. Bai, S., Wang, L., Chen, X., Du, J., Xiong, Y.: Chemically exfoliated metallic MoS_2 nanosheets: a promising supporting co-catalyst for enhancing the photocatalytic performance of TiO_2 nanocrystals. Nano Res. **8**, 175–183 (2015)
201. Lin, Q., Li, L., Liang, S., Liu, M., Bi, J., Wu, L.: Efficient synthesis of monolayer carbon nitride 2D nanosheet with tunable concentration and enhanced visible-light photocatalytic activities. Appl. Catal. B Environ. **163**, 135–142 (2015)
202. Zhu, Y., Ling, Q., Liu, Y., Wang, H., Zhu, Y.: Photocatalytic H_2 evolution on MoS_2–TiO_2 catalysts synthesized via mechanochemistry. Phys. Chem. Chem. Phys. **17**, 933–940 (2015)
203. Zhou, J., Zhang, M., Zhu, Y.: Photocatalytic enhancement of hybrid C_3N_4/TiO_2 prepared via ball milling method. Phys. Chem. Chem. Phys. **17**, 3647–3652 (2015)
204. He, G., Ding, J., Zhang, J., Hao, Q., Chen, H.: One-step ball-milling preparation of highly photocatalytic active $CoFe_2O_4$—reduced graphene oxide heterojunctions for organic dye removal. Ind. Eng. Chem. Res. **54**, 2862–2867 (2015)
205. Liao, L., Zhang, Q., Su, Z., Zhao, Z., Wang, Y., Li, Y., Lu, X., Wei, D., Feng, G., Yu, Q., Cai, X., Zhao, J., Ren, Z., Fang, H., Robles-Hernandez, F., Baldelli, S., Bao, J.: Efficient solar water-splitting using a nanocrystalline CoO photocatalyst. Nat. Nanotechnol. **9**, 69–73 (2014)
206. Choi, Y.I., Jung, H.J., Shin, W.G., Sohn, Y.: Band gap-engineered ZnO and Ag/ZnO by ball-milling method and their photocatalytic and Fenton-like photocatalytic activities. Appl. Surf. Sci. **356**, 615–625 (2015)
207. Merupo, V.I., Velumani, S., Oza, G., Tabellout, M., Bizarro, M., Coste, S., Kassiba, A.H.: High energy ball-milling synthesis of nanostructured Ag-doped and BiVO4-based photocatalysts. Chem. Select. **1**, 1278–1286 (2016)
208. Moghaddam, A.O., Shokuhfar, A., Cabot, A., Zolriasatein, A.: Synthesis of bornite Cu_5FeS_4 nanoparticles via high energy ball milling: photocatalytic and thermoelectric properties. Powder Technol. **333**, 160–166 (2018)
209. Zhao, F., Rong, Y., Wan, J., Hu, Z., Peng, Z., Wang, B.: MoS_2 quantum dots@ TiO_2 nanotube composites with enhanced photo-excited charge separation and high-efficiency visible-light driven photocatalysis. Nanotechnol. **29**, 105403 (2018)
210. Zhong, Y., Shao, Y., Ma, F., Wu, Y., Huang, B., Hao, X.: Band-gap-matched CdSe QD/WS_2 nanosheet composite: size-controlled photocatalyst for high-efficiency water splitting. Nano Energy. **31**, 84–89 (2017)
211. Liu, H., Li, N., Zhang, H., Zhang, F., Su, X.: A simple and convenient fluorescent strategy for the highly sensitive detection of dopamine and ascorbic acid based on graphene quantum dots. Talanta **189**, 190–195 (2018)
212. Sopyan, I., Watanabe, M., Murasawa, S., Hashimoto, K., Fujishima, A.: An efficient TiO_2 thin-film photocatalyst: photocatalytic properties in gas-phase acetaldehyde degradation. J. Photochem. Photobiol. Chemistry. **98**, 79–86 (1996)
213. Zhang, Z., Huang, J., Fang, Y., Zhang, M., Liu, K., Dong, B.: A nonmetal plasmonic Z-scheme photocatalyst with UV-to NIR-driven photocatalytic protons reduction. Adv. Mater. Article ID:1606688, 9 (2017)
214. Leong, K.H., Tan, Z.Z., Sim, L.C., Saravanan, P., Bahnemann, D., Jang, M.: Symbiotic interaction of amalgamated photocatalysts with improved day light utilisation and charge separation. Chem. Select. **2**, 84–89 (2017)
215. Liu, W., Gao, Y., Yang, Y., Zou, Q., Yang, G., Zhang, Z., Li, H., Miao, Y., Li, H., Huo, Y.: Photocatalytic composite of a floating BiOBr@ graphene oxide@ melamine foam for efficient removal of organics. ChemCatChem. **10**, 2394–2400 (2018)
216. Imani, A., Oveisi, H.: 3D-ordered mesoporous chromium-doped titania thin films: the effect of metal dopant on the microstructure, mesoporous symmetry, hydrophobicity, and surface properties. Chem. Select. **3**, 4586–4592 (2018)
217. Arpac, E., Sayılkan, F., Asiltürk, M., Tatar, P., Kiraz, N., Sayılkan, H.: Photocatalytic performance of Sn-doped and undoped TiO_2 nanostructured thin films under UV and vis-lights. J. Hazard. Mater. **140**, 69–74 (2007)
218. Helmy, E.T., El Nemr, A., Mousa, M., Arafa, E., Eldafrawy, S.: Photocatalytic degradation of organic dyes pollutants in the industrial textile wastewater by using synthesized TiO_2, C-doped TiO_2, S-doped TiO_2 and C, S co-doped TiO_2 nanoparticles. J. Water Environ. Nanotechnol. **3**, 116–127 (2018)
219. Sim, L.C., Leong, K.H., Saravanan, P., Ibrahim, S.: Rapid thermal reduced graphene oxide/Pt–TiO_2 nanotube arrays for enhanced visible-light-driven photocatalytic reduction of CO_2. Appl. Surf. Sci. **358**, 122–129 (2015)
220. Weng, L., Zhang, H., Govorov, A. O., Ouyang, M.: Hierarchical synthesis of non-centrosymmetric hybrid nanostructures and enabled plasmon-driven photocatalysis. Nat. Commun. **5**, Article ID: 4792, 10 (2014)
221. Albiter, E., Valenzuela, M.A., Alfaro, S., Valverde-Aguilar, G., Martínez-Pallares, F.M.: Photocatalytic deposition of Ag nanoparticles on TiO_2: metal precursor effect on the structural and photoactivity properties. J. Saudi. Chem. Soc. **19**, 563–573 (2015)
222. Pan, X., Xu, Y.J.: Defect-mediated growth of noble-metal (Ag, Pt, and Pd) nanoparticles on TiO_2 with oxygen vacancies for photocatalytic redox reactions under visible light. J. Phys. Chem. C **117**, 17996–18005 (2013)
223. Subramanian, V., Wolf, E.E., Kamat, P.V.: Catalysis with TiO_2/gold nanocomposites. Effect of metal particle size on the Fermi level equilibration. J. Am. Chem. Soc. **126**, 4943–4950 (2004)
224. Barakat, N.A.M., Kim, H.Y.: Effect of silver-doping on the crystal structure, morphology and photocatalytic activity of TiO_2 nanofibers. In: IOP Conference Series: Mater. Sci. Eng. IOP Publishing. **40**, Article ID: 012003, 7 (2012)
225. Ma, Y., Guan, G., Hao, X., Zuo, Z., Huang, W., Phanthong, P., Li, X., Kusakabe, K., Abudula, A.: Embedded structure catalyst: a new perspective from noble metal supported on molybdenum carbide. RSC Adv. **5**, 15002–15005 (2015)
226. Leong, K.H., Aziz, A.A., Sim, L.C., Saravanan, P., Jang, M., Bahnemann, D.: Mechanistic insights into plasmonic photocatalysts in utilizing visible light. Beilstein J. Nanotechnol. **9**, 628–648 (2018)
227. Castellote, M., Bengtsson, N.: Principles of TiO_2 photocatalysis. In: Ohama Y., Van Gemert D. (eds) Applications of Titanium Dioxide Photocatalysis to Construction Materials, pp. 5–10. Springer, Dordrecht (2011)
228. Schneider, J., Matsuoka, M., Takeuchi, M., Zhang, J., Horiuchi, Y., Anpo, M., Bahnemann, D.W.: Understanding TiO_2 photocatalysis: mechanisms and materials. Chem. Rev. **114**, 9919–9986 (2014)
229. Tiwari, A., Krishna, N.V., Giribabu, L., Pal, U.: Hierarchical porous TiO_2 embedded unsymmetrical zinc-phthalocyanine sensitizer for visible-light-induced photocatalytic H_2 production. J. Phys. Chem. C. **122**, 495–502 (2018)
230. Okamoto, Y., Ida, S., Hyodo, J., Hagiwara, H., Ishihara, T.: Synthesis and Photocatalytic activity of rhodium-doped calcium niobate nanosheets for hydrogen production from a water/methanol system without cocatalyst loading. J. Am. Chem. Soc. **133**, 18034–18037 (2011)
231. Hu, Y., Guo, L.: Rapid preparation of perovskite lead niobate nanosheets by ultrasonic-assisted exfoliation for enhanced visible-light-driven photocatalytic hydrogen production. ChemCatChem. **7**, 584–587 (2015)
232. Maeda, K., Eguchi, M., Oshima, T.: Perovskite oxide nanosheets with tunable band-edge potentials and high photocatalytic

hydrogen-evolution activity. Angew. Chem. Int. Ed. **53**, 13164–13168 (2014)
233. Luo, P.G., Sahu, S., Yang, S.T., Sonkar, S.K., Wang, J., Wang, H., Lecroy, G.E., Cao, Li., Sun, Y.P.: Carbon "quantum" dots for optical bioimaging. J. Mater. Chem. B. **1**, 2116–2127 (2013)
234. Luo, P.G., Yang, F., Yang, S.T., Sonkar, S.K., Yang, L., Broglie, J.J., Liu, Y., Sun, Y.P.: Carbon-based quantum dots for fluorescence imaging of cells and tissues. RSC Adv. **4**, 10791–10807 (2014)
235. Sahu, S., Liu, Y., Wang, P., Bunker, C. E., Shiral Fernando, K. A., Lewis, W. K., Guliants, E.A., Yang, F., Wang, J., Sun, Y.P.: Visible-light photoconversion of carbon dioxide into organic acids in an aqueous solution of carbon dots. Langmuir : ACS J. Surf. Coll. **30**, 8631–8636 (2015)
236. Cao, L., Meziani, M.J., Sahu, S., Sun, Y.P.: Photoluminescence properties of graphene versus other carbon nanomaterials. Acc. Chem. Res. **46**, 171–180 (2013)
237. Liu, J., Zhang, Y., Lu, L., Wu, G., Chen, W.: Self-regenerated solar-driven photocatalytic water-splitting by urea derived graphitic carbon nitride with platinum nanoparticles. Chem. Commun. **48**, 8826–8828 (2012)
238. Liu, J., Liu, Y., Liu, N., Han, Y., Zhang, X., Huang, H., Lifshitz, Y., Lee, S.T., Zhong, J., Kang, Z.: Metal-free efficient photocatalyst for stable visible water splitting via a two-electron pathway. Science **347**, 970–974 (2015)
239. Shinde, S.L., Ishii, S., Dao, T.D., Sugavaneshwar, R.P., Takei, T., Nanda, K.K., Nagao, T.: Enhanced solar light absorption and photoelectrochemical conversion using TiN nanoparticle-incorporated C_3N_4-C dot sheets. ACS Appl. Mater. Interfaces. **10**, 2460–2468 (2018)
240. Chowdhury, S., Balasubramanian, R.: Graphene/semiconductor nanocomposites (GSNs) for heterogeneous photocatalytic decolorization of wastewaters contaminated with synthetic dyes : a review. Appl. Catal. B: Environ. **160**, 307–324 (2014)
241. Mateo, D., Esteve-Adell, I., Albero, J., Primo, A., García, H.: Oriented 2.0.0 Cu_2O nanoplatelets supported on few-layers graphene as efficient visible light photocatalyst for overall water splitting. Appl. Catal. B: Environ. . **201**, 582–590 (2017)
242. Habisreutinger, S.N., Schmidt-Mende, L., Stolarczyk, J.K.: Photocatalytic reduction of CO_2 on TiO_2 and other semiconductors. Angew. Chem. Int. Ed. **52**, 7372–7408 (2013)
243. Lin, J., Pan, Z., Wang, X.: Photochemical reduction of CO_2 by graphitic carbon nitride polymers. ACS Sustain. Chem. Eng. **2**, 353–358 (2014)
244. Shoji, S., Yamaguchi, A., Sakai, E., Miyauchi, M.: Strontium titanate-based artificial leaf loaded with reduction and oxidation cocatalysts for selective CO_2 reduction using water as an electron donor. ACS Appl. Mater. Interfaces. **9**, 20613–20619 (2017)
245. Zhou, J., Chen, W., Sun, C., Han, L., Qin, C., Chen, M., Wang, X., Wang, E., Su, Z.: Oxidative polyoxometalates modified graphitic carbon nitride for visible-light CO_2 reduction. ACS Appl. Mater. Interfaces. **9**, 11689–11695 (2017)
246. Morimoto, T., Nishiura, C., Tanaka, M., Rohacova, J., Nakagawa, Y., Funada, Y., Koike, K., Yamamoto, Y., Shishido, S., Kojima, T., Saeki, T., Ozeki, T., Ishitani, O.: Ring-shaped Re(I) multinuclear complexes with unique photofunctional properties. J. Am. Chem. Soc. **135**, 13266–13269 (2013)
247. Wang, W.N., Wu, F., Myung, Y., Niedzwiedzki, D.M., Im, H.S., Park, J., Banerjee, P., Biswas, P.: Surface engineered CuO nanowires with ZnO Islands for CO_2 photoreduction. ACS Appl. Mater. Interfaces. **7**, 5685–5692 (2015)
248. Ali, A., Oh, W.: Preparation of nanowire like WSe_2—graphene nanocomposite for photocatalytic reduction of CO_2 into CH_3OH with the presence of sacrificial agents. Sci. Rep. **7**, Article ID: 1867, 11 (2017)
249. Yosefi, L., Haghighi, M.: Fabrication of nanostructured flower-like p-BiOI/p-NiO heterostructure and its efficient photocatalytic performance in water treatment under visible-light irradiation. Appl. Catal. B: Environ. **220**, 367–378 (2018)
250. Kumar, A., Khan, M., Fang, L., Lo, I. M.: Visible-light-driven N-TiO_2@ SiO_2@ Fe_3O_4 magnetic nanophotocatalysts: synthesis, characterization, and photocatalytic degradation of PPCPs. J. Hazard. Mater. Article ID: 18740, 9 (2017) **(in press)**
251. Jiménez-Tototzintle, M., Oller, I., Hernández-Ramírez, A., Malato, S., Maldonado, M.I.: Remediation of agro-food industry effluents by biotreatment combined with supported TiO_2/H_2O_2 solar photocatalysis. Chem. Eng. J. **273**, 205–213 (2015)
252. Mansur, A.A., Mansur, H.S., Ramanery, F.P., Oliveira, L.C., Souza, P.P.: "Green" colloidal ZnS quantum dots/chitosan nanophotocatalysts for advanced oxidation processes: study of the photodegradation of organic dye pollutants. Appl. Catal. B: Environ. **158**, 269–279 (2014)
253. Kumar, A., Sharma, G., Naushad, M., Kumar, A., Kalia, S., Guo, C., Mola, G.T.: Facile hetero-assembly of superparamagnetic Fe_3O_4/$BiVO_4$ stacked on biochar for solar photo-degradation of methyl paraben and pesticide removal from soil. J. Photochem. Photobiol. A Chem. **337**, 118–131 (2017)
254. Hu, X., Li, G., Yu, J.C.: Design, fabrication, and modification of nanostructured semiconductor materials for environmental and energy applications. Langmuir **26**, 3031–3039 (2010)
255. Lee, S.W., Cheon, S.A., Kim, M., Park, T.J.: Organic-inorganic hybrid nanoflowers: types, characteristics, and future prospects. J. Nanobiotechnol. **13**, 5–10 (2015)
256. Tian, J., Zhao, Z., Kumar, A., Boughton, R.I., Liu, H.: Recent progress in design, synthesis, and applications of one-dimensional TiO_2 nanostructured surface heterostructures: a review. Chem. Soc. Rev. **43**, 6920–6937 (2014)
257. Zhou, H., Li, P., Liu, J., Chen, Z., Liu, L., Dontsova, D., Ye, J.: Biomimetic polymeric semiconductor based hybrid nanosystems for artificial photosynthesis towards solar fuels generation via CO_2 reduction. Nano Energy. **25**, 128–135 (2016)
258. Zhang, L., Martin, A., Perry, M.W., Van Der Burg, K.R.L., Matsuoka, Y., Monteiro, A., Reed, R.D.: Genetic basis of melanin pigmentation in butterfly wings. Genetics **205**, 1537–1550 (2017)
259. Stavenga, D. G., Leertouwer, H. L., Meglic, A., Draslar, K., Wehling, M. F., Pirih, P., Belusic, G.: Classical lepidopteran wing scale colouration in the giant butterfly-moth Paysandisia archon. Peer J. Article ID:4590, 18 (2018)
260. Siddique, R.H., Donie, Y.J., Gomard, G., Lemmer, U., Hölscher, H.: Bio-inspired Black Butterfly's Wing Nanostructures for Absorption Enhancement in Solar Cells. IONS Karlsruhe (2015)
261. Narasimhan, V., Siddique, R.H., Lee, J.O., Kumar, S., Ndjamen, B., Du, J., Choo, H.: Multifunctional biophotonic nanostructures inspired by the longtail glasswing butterfly for medical devices. Nat. Nanotechnol. **13**, 512–519 (2018)
262. Ma, Z., Zhang, Y.L., Wang, L., Ming, H., Li, H., Zhang, X., Lee, S.T.: Bioinspired photoelectric conversion system based on carbon-quantum-dot- doped dye-semiconductor complex. ACS Appl. Mater. Interfaces. **5**, 5080–5084 (2013)
263. Fu, J., Zhu, B., You, W., Jaroniec, M., Yu, J.: A flexible bio-inspired H_2-production photocatalyst. Appl. Catal. B: Environm. **220**, 148–160 (2018)
264. Ye, S., Ding, C., Chen, R., Fan, F., Fu, P., Yin, H., Li, C.: Mimicking the key functions of photosystem II in artificial photosynthesis for photoelectrocatalytic water splitting. J. Am. Chem. Soc. **140**, 3250–3256 (2018)
265. Saer, R.G., Blankenship, R.E.: Light harvesting in phototrophic bacteria: structure and function. Biochem. J. **474**, 2107–2131 (2017)

266. Liu, J., Antonietti, M.: Bio-inspired NADH regeneration by carbon nitride photocatalysis using diatom templates. Energ. Environ. Sci. **6**, 1486–1493 (2013)
267. Wei, J., Xu, R.P., Li, Y.Q., Li, C., Chen, J.De, Zhao, X.D., Tang, J.X.: Enhanced light harvesting in perovskite solar cells by a bioinspired nanostructured back electrode. Adv. Energy Mater. **7**, 1–7 (2017)
268. Behera, S., Joseph, J.: Single-step optical realization of bio-inspired dual-periodic motheye and gradient-index-array photonic structures. Opt. Lett. **41**, 3579–3582 (2016)
269. Arora, N., Sharma, N.N.: Arc discharge synthesis of carbon nanotubes: comprehensive review. Diamond Relat. Mater. **50**, 135–150 (2014)
270. Jeong, S.H., Ko, J.H., Park, J.B., Park, W.: A sonochemical route to single-walled carbon nanotubes under ambient conditions. J. Am. Chem. Soc. **126**, 15982–15983 (2004)
271. Coroş, M., Pogăcean, F., Roşu, M.C., Socaci, C., Borodi, G., Mageruşan, L., Biriş, A.R., Pruneanu, S.: Simple and cost-effective synthesis of graphene by electrochemical exfoliation of graphite rods. RSC Adv. **6**, 2651–2661 (2016)
272. Kondalkar, V.V., Kharade, R.R., Mali, S.S., Mane, R.M., Patil, P.B., Patil, P.S., Choudhury, S., Bhosale, P.N.: Nanobrick-like WO_3 thin films: hydrothermal synthesis and electrochromic application. Superlattices Microstruct. **73**, 290–295 (2014)
273. Walton, R.I.: Subcritical solvothermal synthesis of condensed inorganic materials. Chem. Soc. Rev. **31**, 230–238 (2002)
274. Li, H., Shao, F.Q., Zou, S.Y., Yang, Q.J., Huang, H., Feng, J.J., Wang, A.J.: Microwave-assisted synthesis of N, P-doped carbon dots for fluorescent cell imaging. Microchim. Acta **183**, 821–826 (2016)
275. Bhattarai, N., Khanal, S., Velazquez-Salazar, J.J., Jose-Yacaman, M.: Advanced electron microscopy in the study of multimetallic nanoparticles. In: Deepak, F., Mayoral, A., Arenal, R. (eds.) Advanced Transmission Electron Microscopy, pp. 59–91. Springer, Cham (2015)
276. Hussain, S., Akbar, K., Vikraman, D., Choi, D.C., Kim, S.J., An, K.S., Jung, S., Jung, J.: A highly sensitive enzymeless glucose sensor based on 3D graphene–Cu hybrid electrodes. New J. Chem. **39**, 7481–7487 (2015)
277. Hafshejani, L.D., Tangsir, S., Koponen, H., Riikonen, J., Karhunen, T., Tapper, U., Lehto, V.P., Moazed, H., Naseri, A.A., Hooshmand, A., Jokiniemi, J., Bhatnagar, A., Lahde, A.: Synthesis and characterization of Al_2O_3 nanoparticles by flame spray pyrolysis (FSP)—role of Fe ions in the precursor. Powder Technol. **298**, 42–49 (2016)
278. Zori, M.H.: Synthesis of TiO_2 nanoparticles by microemulsion/heat treated method and photodegradation of methylene blue. J. Inorg. Organomet. Polym Mater. **21**, 81–90 (2011)
279. Owens, G.J., Singh, R.K., Foroutan, F., Alqaysi, M., Han, C.M., Mahapatra, C., Kim, H.W., Knowles, J.C.: Sol–gel based materials for biomedical applications. Prog. Mater Sci. **77**, 1–79 (2016)
280. Pavithra, C.L., Sarada, B.V., Rajulapati, K.V., Rao, T.N., Sundararajan, G.: A new electrochemical approach for the synthesis of copper-graphene nanocomposite foils with high hardness. Sci. Rep. **4**, Article ID: 4049, 7 (2014)
281. Lai, Y., Sun, L., Chen, Y., Zhuang, H., Lin, C., Chin, J.W.: Effects of the structure of TiO_2 nanotube array on Ti substrate on its photocatalytic activity. J. Electrochem. Soc. **153**, D123–D127 (2006)
282. Malkhasian, A.Y., Narasimharao, K.: Structural and photocatalytic properties of Pd-deposited semiconductors with different morphology. RSC Adv. **7**, 55633–55645 (2017)
283. Zhang, L., Xu, T., Zhao, X., Zhu, Y.: Controllable synthesis of Bi_2MoO_6 and effect of morphology and variation in local structure on photocatalytic activities. Appl. Catal. B: Environ. **98**, 138–146 (2010)
284. Guo, M., He, Q., Wang, W., Wu, J., Wang, W.: Fabrication of $BiVO_4$: Effect of structure and morphology on photocatalytic activity and its methylene blue decomposition mechanism. J. Wuhan Univ. Technol. Mater. Sci. Ed. **31**, 791–798 (2016)
285. Yu, J., Kudo, A.: Effects of structural variation on the photocatalytic performance of hydrothermally synthesized $BiVO_4$. Adv. Funct. Mater. **16**, 2163–2169 (2006)
286. Teeparthi, S.R., Awin, E. W., Kumar, R.: Dominating role of crystal structure over defect chemistry in black and white zirconia on visible light photocatalytic activity. Sci. Rep. **8**, Article ID:5541, 11 (2018)
287. Nagy, D., Szilágyi, I.M., Firkala, T., Xianfeng, F.: Study about the morphology effect on the photo-efficiency of WO_3. Eur. Chem. Bull. **5**, 40–42 (2016)
288. Tachikawa, T., Fujitsuka, M., Majima, T.: Mechanistic insight into the TiO_2 photocatalytic reactions: design of new photocatalysts. J. Phys. Chem. C **111**, 5259–5275 (2007)
289. Chakravarty, M., Das, A., Sarma, C., Roy, P.: α-Fe_2O_3/TiO_2 hybrids with tunable morphologies as efficient photocatalysts and positive electrodes for supercapacitors. Chem. Select. **3**, 3284–3294 (2018)
290. Xu, D., Cao, S., Zhang, J., Cheng, B., Yu, J.: Effects of the preparation method on the structure and the visible-light photocatalytic activity of Ag_2CrO_4. Beilstein J. Nanotechnol. **5**, 658–666 (2014)
291. Kegel, J., Zubialevich, V.Z., Schmidt, M., Povey, I.M., Pemble, M.E.: Effect of surface and defect chemistry on the photo-catalytic properties of intentionally defect-rich ZnO nanorod arrays. ACS Appl. Mater. Interfaces. **10**, 17994–18004 (2018)
292. Ma, X., Li, X., Li, M., Ma, X., Yu, L., Dai, Y.: Effect of the structure distortion on the high photocatalytic performance of C_{60}/g-C_3N_4 composite. Appl. Surf. Sci. **414**, 124–130 (2017)
293. Huo, Y., Hou, R., Chen, X., Yin, H., Gao, Y., Li, H.: BiOBr visible-light photocatalytic films in a rotating disk reactor for the degradation of organics. J. Mater. Chem. A. **3**, 14801–14808 (2015)
294. Ding, S., Liu, X., Shi, Y., Liu, Y., Zhou, T., Guo, Z., Hu, J.: Generalized synthesis of ternary sulfide hollow structures with enhanced photocatalytic performance for degradation and hydrogen evolution. ACS Appl. Mater. Interfaces. **10**, 17911–17922 (2018)
295. Zhao, T., Liu, Z., Nakata, K., Nishimoto, S., Murakami, T., Zhao, Y., Jiang, L., Fujishima, A.: Multichannel TiO_2 hollow fibers with enhanced photocatalytic activity. J. Mater. Chem. **20**, 5095–5099 (2010)
296. Li, H., Bian, Z., Zhu, J., Zhang, D., Li, G., Huo, Y., Li, H., Lu, Y.: Mesoporous titania spheres with tunable chamber structure and enhanced photocatalytic activity. J. Am. Chem. Soc. **129**, 8406–8407 (2007)
297. Angkaew, S., Limsuwan, P.: Preparation of silver-titanium dioxide core-shell (Ag@ TiO_2) nanoparticles: effect of Ti-Ag mole ratio. Procedia Eng. **32**, 649–655 (2012)
298. Wang, D., Hisatomi, T., Takata, T., Pan, C., Katayama, M., Kubota, J., Domen, K.: Core/Shell photocatalyst with spatially separated co-catalysts for efficient reduction and oxidation of water. Angew. Chem. Int. Ed. **52**, 11252–11256 (2013)
299. Kim, C., Cho, K.M., Al-Saggaf, A., Gereige, I., Jung, H.T.: Z-scheme photocatalytic CO_2 conversion on three-dimensional $BiVO_4$/carbon-coated Cu_2O nanowire arrays under visible light. ACS Catal. **8**, 4170–4177 (2018)
300. Ahn, C.W., Borse, P.H., Kim, J.H., Kim, J.Y., Jang, J.S., Cho, C.R., Yoon, J.H., Lee, B., Bae, J.S., Kim, H.G., Lee, J.S.: Effective charge separation in site-isolated Pt-nanodot deposited $PbTiO_3$ nanotube arrays for enhanced photoelectrochemical water splitting. Appl. Catal. B: Environ. **224**, 804–809 (2018)

301. Sun, X., Mi, Y., Jiao, F., Xu, X.: Activating layered perovskite compound Sr_2TiO_4 via La/N codoping for visible light photocatalytic water splitting. ACS Catal. **8**, 3209–3221 (2018)
302. Chiang, T.H., Lyu, H., Hisatomi, T., Goto, Y., Takata, T., Katayama, M., Minegishi, T., Domen, K.: Efficient photocatalytic water splitting using Al-doped $SrTiO_3$ coloaded with molybdenum oxide and rhodium-chromium oxide. ACS Catal. **8**, 2782–2788 (2018)
303. Sakata, Y., Hayashi, T., Yasunaga, R., Yanaga, N., Imamura, H.: Remarkably high apparent quantum yield of the overall photocatalytic H_2O splitting achieved by utilizing Zn ion added Ga_2O_3 prepared using dilute $CaCl_2$ solution. Chem. Commun. **51**, 12935–12938 (2015)
304. Tian, B., Tian, B., Smith, B., Scott, M. C., Hua, R., Lei, Q., Tian, Y.: Supported black phosphorus nanosheets as hydrogen-evolving photocatalyst achieving 5.4% energy conversion efficiency at 353 K. Nat. Commun. **9**, 1–11 (2018)
305. Kumar, A., Prajapati, P.K., Pal, U., Jain, S.L.: A ternary rGO/InVO4/Fe_2O_3 Z-scheme heterostructured photocatalyst for CO_2 reduction under visible light irradiation. ACS Sustain. Chem. Eng. **6**, 8201–8211 (2018)
306. Xu, Y.F., Yang, M.Z., Chen, B.X., Wang, X.D., Chen, H.Y., Kuang, D.B., Su, C.Y.: A $CsPbBr_3$ perovskite quantum dot/graphene oxide composite for photocatalytic CO_2 reduction. J. Am. Chem. Soc. **139**, 5660–5663 (2017)

Publisher's Note Springer Nature remains neutral with regard to jurisdictional claims in published maps and institutional affiliations.